CLASSICAL PHASE DIAGRAM OF KITAEV-HEISENBERG MODEL ON KAGOME LATTICE

A THESIS
SUBMITTED TO THE FACULTY OF THE GRADUATE SCHOOL
OF THE UNIVERSITY OF MINNESOTA
BY

FULYA KOC

IN PARTIAL FULFILLMENT OF THE REQUIREMENTS
FOR THE DEGREE OF
MASTER OF SCIENCE

NATALIA PERKINS

June, 2016

Acknowledgements

I would like to begin by acknowledging the tremendous help and guidance from my advisers Prof. Natalia Perkins and Dr. Ioannis Rousochatzakis, it has been a great privilege to be advised by them through the course of my MSc research. Natalia and Ioannis have been true mentors for me both regarding to the physics and overall life experiences. I appreciate their patience and support in all respects. I would like to thank them for helping me to acquire a deeper knowledge of physics and let me understand all the phenomena as well as technical details regarding to my research topic.

I am also grateful to Prof. Jorge Vinals and to Prof. Elias Puchner, who served as my committee members, for their time and consideration, and all valuable suggestions for improvements.

I further would like to thank to my friend You Jhih-Shih for all his support throughout this time period. I am grateful for the discussions we made regardless of time and distance. All his suggestions helped me to broaden my perspective in physics. Additionally, I would like to thank to my colleague Yuriy Sizyuk for all his help, clear explanations and welcoming approach for all of my questions. I am happy to know him and be able to benefit from his experiences.

Finally, I would like to thank to my parents for all their supports and encouragements throughout the whole thesis process. I feel incredibly lucky to have them in my life.

Abstract

We study the classical ground states of the nearest-neighbor Kitaev-Heisenberg Hamiltonian on the kagome lattice using the Luttinger-Tizsa method and the canonical three sublattice transformation. We have computed classical phase diagram of the model. We analyzed the structure of all magnetic states entering to this phase diagram. We observed that some of the phases carry highly degenerate ground state manifolds because of the frustrated nature of the model system. In the future work we plan to study the role of farther neighbor interactions, and the effects of finite temperature with quantum fluctuations.

Contents

List of Figures

Chapter 1

Introduction

1.1 Magnetic interactions in correlated materials with strong spin-orbit coupling

In correlated electron systems, frustration and competing energy scales often leads to novel quantum and classical phases and novel properties. In particular interesting are magnetic properties of such systems.In some magnetic compounds containing 5d transition metal ions [6,10], i.e. iridates and osmates, relativistic spin-orbit coupling (SOC) becomes comparable with Coulomb interaction and crystal fields. This is why the magnetic properties of 5d transition metal oxides are very different from those of 3d systems, in which Coulomb interaction and crystal fields are dominant interactions, and SOC can be treated as a perturbation, whose main role is to give rise to a magnetic anisotropy of either an easy-axis or an easy-plane type. In 5d-systems, SOC can not be treated as perturbation.In addition, the form of magnetic interactions is not dictated by spin symmetry alone, instead, the symmetry of the low-energy the Hamiltonians is determined by the combination of spin and lattice symmetries.

For instance, the magnetic Hamiltonians might contain terms that are products of different components of multiple spin operators. Such terms, which aren't allowed in the traditionally studied SU(2) symmetric models, introduce a new source of frustration [25, 26], and as a result one can observe novel types of ground states. The Kitaev honeycomb lattice model [18], describing a very particular interaction of spin-1/2 moments can be

given as an example of such a behavior in which its low energy state is can be solved exactly and known as a spin liquid.

Some of these anisotropic models can be realized in real materials. It has been suggested that A_2IrO_3 compounds, where A is an alkali metal ion, can be described with the Kitaev-Heisenberg (KH) model on the honeycomb lattice [5,28]. Due to strong SOC, the atomic ground state forms a doublet where the spin and orbital angular momenta of Ir^{4+} ions are coupled into $J_{eff} = 1/2$. It has been suggested [29] that the interactions between these effective spin$-1/2$ moments can be described by a spin Hamiltonian containing two competing nearest neighbor interactions; i.e. an isotropic antiferromagnetic (AFM) Heisenberg exchange and a highly anisotropic bond directional ferromagnetic (FM) exchange [9, 12, 29]. The competition between these two limits can be described by a single parameter, $0 \leq \alpha \leq 1$, which sets the relative strength of these two interactions. At $\alpha = 0$, the coupling between the moments of Ir ions corresponds to the AFM Heisenberg interaction; while at $\alpha = 1$, it corresponds to the FM Kitaev interaction. Previous studies of the ground state properties of the KH model have shown that it has a very rich phase diagram [7, 8, 17, 28]. The KH model on the honeycomb lattice exhibits three distinct phases: the AFM Neel phase, the stripy AFM phase, and the disordered spin-liquid phase, see Fig.1.1 for phase diagram as presented in paper of Chaloupka et al. [4] .

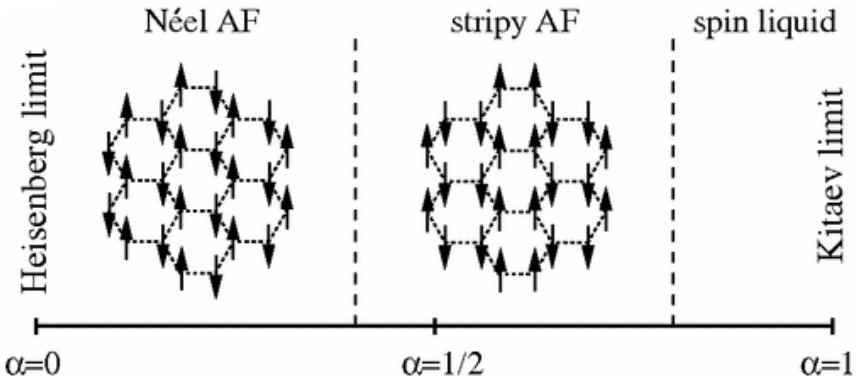

Figure 1.1: Schematic phase diagram of KH model on honeycomb lattice. As the parametrization value α increases, the ground state changes from the Néel FM to the Kitaev spin liquid. [4].

In this thesis, we will study the Kitaev-Heisenberg model on the kagome lattice, where the Kitaev part of the Hamiltonian can also be considered as an example of a compass model, as the associated bond-directional couplings take precisely the form of a compass Hamiltonian, originally introduced in the context of spin-orbital compounds by K. I. Kugel and D. I. Khomskii [19].

Recent years, kagome lattice compounds in particular containing $S = 1/2$ ions, for instance Cu^{2+} and V^{4+}, attracted a lot of attention as the quantum fluctuations can compete with the tendency towards long-range magnetic order and leading to novel magnetic ground states such as quantum spin liquids [11]. Quantum spin liquids cannot be described by the broken symmetries associated with conventional ground states as the interacting magnetic moments in these systems are highly entangled with each other over the long ranges [2], and they have a prominent role in describing the high-T_c superconductors [1, 20] and their topological features might offer some applications in the field of quantum information theory [13].

Kitaev-Heisenberg model on kagome lattice is well known to provide one of the

most frustrated lattice topologies due to both the isotropic Heisenberg term and the anisotropic Kitaev term, so before we give the precise form of Hamiltonian we will first discuss what we mean by frustration.

1.2 Frustration

There are basically two types of frustration; one is due to geometry, and the other is due to competing interactions.

Geometrical frustration occurs as a result of the lattice geometry. Meaning, due to the topology of the lattice, not all interactions are simultaneously satisfied. Hence, one will obtain degenerate manifold of ground states. This type of frustration can be seen in lattices having triangular basis.

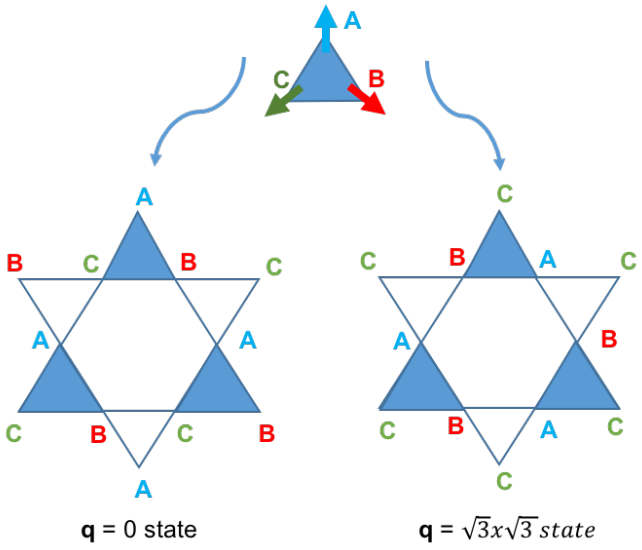

Figure 1.2: Two of the infinitely many degenerate ground state configurations belonging to the anti-ferromagnetic Heisenberg point. Left corresponds to the $\mathbf{q} = 0$ state and right corresponds to the $\mathbf{q} = \sqrt{3} \times \sqrt{3}$ state. This is to illustrate the frustration in the Heisenberg part.

As we can see on Fig.1.2, kagome lattice is made of corner sharing triangles and all of the spins make 120^o with each other in each triangle to satisfy ground state condition, which we will discuss in detail in Section 3.4.2. On the Fig.1.2, one can see two different spin configurations, $\mathbf{q} = 0$ and $\mathbf{q} = \sqrt{3} \times \sqrt{3}$ respectively, which are degenerate with each other. There are many other spin configurations satisfying 120^o condition, but for the purpose of illustration, we chose only two of them. We can see many other examples of such frustration, for instance, in triangular lattice or 3D pyrochlore lattice.

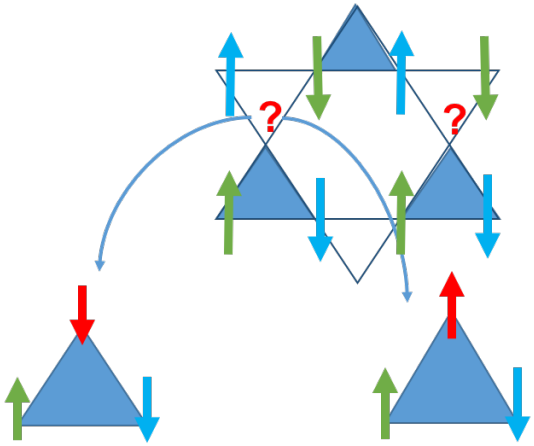

Figure 1.3: Two of the possible highly degenerate ground state configurations belonging to the anti-ferromagnetic Kitaev point. This is to illustrate the frustration in Kitaev part.

Another type of frustration occurs due to the bond directional character of the Ising-like competing interactions as one can see on Fig1.3. There are three types of n.n. bonds, and n.n. spins interact with Ising like interactions where S^xS^x on the xx-type, S^yS^y on the yy-type, and S^zS^z on the zz-type of bonds. All the bond directions are degenerate with each other, see section 3.4.1.6, so we can choose any of the three, i.e. let's pick zz bond and place the spins anti-ferromagnetically along the z-axis. Question marks on the intersections of xx and yy bonds represents dangling spins. That is to say, one has freedom to choose the spin direction as up or down because any configuration on these intersections are degenerate with each other and spin flipping cost no additional

energy.

As one can see in Fig1.2 and Fig1.3, KH model on kagome lattice combines both types of frustration. Geometric frustration occurs due to the Heisenberg term in the Hamiltonian, while frustration due to the interaction occurs in the bond-directional Ising interactions in the Kitaev term.

Before we describe our model in detail, it's important to mention that magnetic states occurring in KH model aren't always collinear. Actually, there are many other interesting magnetically ordered states like coplanar and non-coplanar states depending on which interaction is favored.

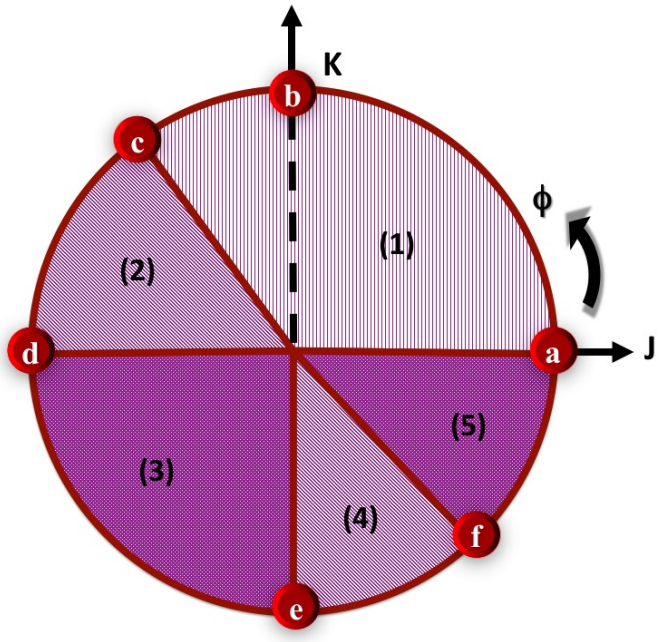

Figure 1.4: Classical phase diagram for Kitaev-Heisenberg model on Kagome lattice with parametrization $K = sin(\phi)$ and $J = cos(\phi)$, where ϕ is the parametrization angle s.t. $\phi\epsilon[0, 2\pi]$.

Fig.1.4 shows the main result of my thesis - the classical phase diagram of Kitaev-Heisenberg model on kagome lattice. The angle ϕ parametrizes the strengths of the two

interactions of the model, the Heisenberg $J = \cos(\phi)$ and the Kitaev $K = \sin(\phi)$.

The phase diagram contains five (1-5) extended phases, and six (a-f) special isolated points:

(1) $\vec{q} = 0$ coplanar AFM states,

(2) $\vec{q} = 0$ non-coplanar states,

(3) The uniform $\vec{q} = 0$ FM state,

(4) $\vec{q} = 0$ dual-non-coplanar states, and

(5) The dual $\vec{q} = 0$ FM state.

(a) Heisenberg antiferromagnetic (HAFM) point, $\phi = 0$,

(b) Kitaev antiferromagnetic (KAFM) point, $\phi = \pi/2$,

(c) The dual-HAF point, $\phi = arctan(-2) + \pi$,

(d) Heisenberg Ferromagnetic (HFM) point, $\phi = \pi$,

(e) Kitaev Ferromagnetic (KFM) point, $\phi = 3\pi/2$, and

(f) The dual-HFM point, $\phi = arctan(-2)$.

The extended phases (1), (2), and (4) consists of 8 distinct, symmetry equivalent states, while the FM phase (3) and the dual-FM phase (5) have an accidental SO(3) degeneracy, not related to symmetry, except at the special points $\phi = \pi$ (d) and $\phi = -arctan(2)$ (f) where the model becomes SO(3) symmetric in a special rotated frame.

The remaining four special isolated points also have high degeneracy; The HAFM point, (a), and the dual-HAFM point, (c), have a continuous degeneracy related to the SO(3) symmetry, as well as an additional infinite degeneracy which is accidental. This is a well known property of the classical Heisenberg model on the kagome lattice [7,8]. The Kitaev points (b) and (e) have a sub-extensive number of ground states related to a special symmetry of the Hamiltonian at these special points.

In the following, we will discuss these phases in detail after we introduce the model and the methods we have used to compute the phase diagram.

Chapter 2

The Model

2.1 Hamiltonian

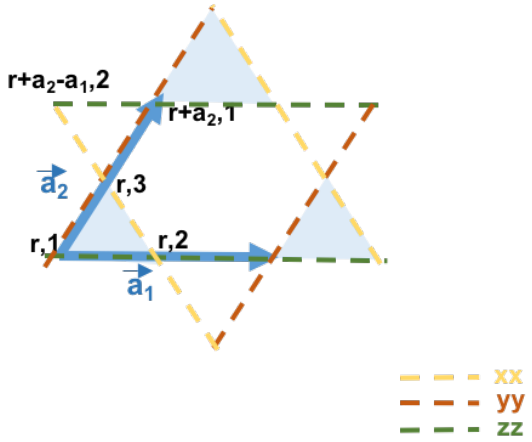

Figure 2.1: Kagome lattice with its xx,yy and zz bonds. Each unit cell contains three different classical spin vectors.

Kagome lattice is a triangular Bravais lattice with a unit cell of three sites. We label the sites with $(\mathbf{r}, n)$, where $\mathbf{r}$ denotes the position of the unit cell and $n = 1, 2, 3$ denotes the sublattice index. Then, the Kitaev-Heisenberg model can be written as

$$\begin{aligned}\hat{H} &= J\sum_{\mathbf{r}}[(\mathbf{S}_{\mathbf{r},1}\cdot\mathbf{S}_{\mathbf{r},2}+\mathbf{S}_{\mathbf{r},1}\cdot\mathbf{S}_{\mathbf{r},3}+\mathbf{S}_{\mathbf{r},2}\cdot\mathbf{S}_{\mathbf{r},3}) \\ &+ (\mathbf{S}_{\mathbf{r}+\mathbf{a}_2,1}\cdot\mathbf{S}_{\mathbf{r}+\mathbf{a}_2-\mathbf{a}_1,2}+\mathbf{S}_{\mathbf{r}+\mathbf{a}_2,1}\cdot\mathbf{S}_{\mathbf{r},3}+\mathbf{S}_{\mathbf{r}+\mathbf{a}_2-\mathbf{a}_1,2}\cdot\mathbf{S}_{\mathbf{r},3})] \\ &+ K\sum_{\mathbf{r}}[(S^x_{\mathbf{r},2}S^x_{\mathbf{r},3}+S^x_{\mathbf{r},3}S^x_{\mathbf{r}+\mathbf{a}_2-\mathbf{a}_1,2})+(S^y_{\mathbf{r},1}S^y_{\mathbf{r},3}+S^y_{\mathbf{r}+\mathbf{a}_2,1}S^y_{\mathbf{r},3}) \\ &+ (S^z_{\mathbf{r},1}S^z_{\mathbf{r},2}+S^z_{\mathbf{r}+\mathbf{a}_2,1}S^z{}_{\mathbf{r}+\mathbf{a}_2-\mathbf{a}_1,2})].\end{aligned} \tag{2.1.1}$$

Whole lattice space can be spanned by the primitive lattice vectors $\mathbf{a}_1 = (1, 0)$ and $\mathbf{a}_2 = \left(\frac{1}{2}, \frac{\sqrt{3}}{2}\right)$.

2.2 Brillouin zone

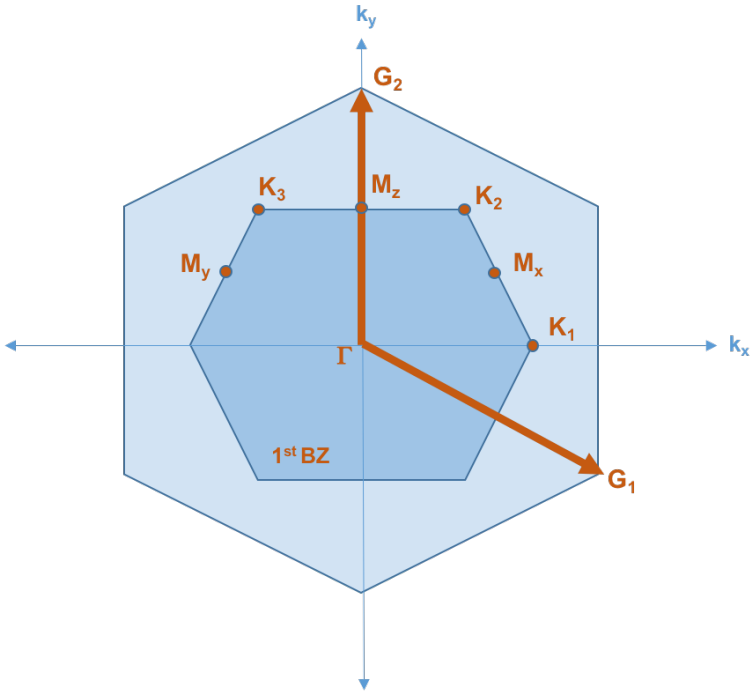

Figure 2.2: The first BZ of the kagome lattice is the inner (darker) hexagon, along with special momenta points.

One can see the Brillouin zone (BZ) of kagome lattice in Fig. 2.2, where we define the reciprocal lattice vectors as $\mathbf{G}_1 = (2\pi, -\frac{2\pi}{\sqrt{3}})$ and $\mathbf{G}_2 = (0, \frac{4\pi}{\sqrt{3}})$. Additionally, some other special points of the 1st BZ are

$$\begin{aligned} \mathbf{K}_1 &= \left(\frac{4\pi}{3}, 0\right), \ \mathbf{K}_2 = \left(\frac{2\pi}{3}, \frac{2\pi}{\sqrt{3}}\right), \ \mathbf{K}_3 = \left(-\frac{2\pi}{3}, \frac{2\pi}{\sqrt{3}}\right) \\ \mathbf{M}_x &= \left(\pi, \frac{\pi}{\sqrt{3}}\right), \ \mathbf{M}_y = \left(-\pi, \frac{\pi}{\sqrt{3}}\right), \mathbf{M}_z = \left(0, \frac{2\pi}{\sqrt{3}}\right) \\ \Gamma &= (0,0)\,. \end{aligned} \tag{2.2.1}$$

Chapter 3

Luttinger-Tizsa Method

3.1 General method

The Luttinger-Tisza (LT) method is a method for finding the ordering wavevector that characterizes the lowest energy state of the model Hamiltonian for a given set of interactions. Our main goal is to find the ground states of the model Hamiltonian (2.1.1),i.e., to find the set of N spins S_i which minimize the total energy subject to the constraint that all of the spins have unit length, the so-called strong constraint [16, 22, 23], which is in real space and in momentum space respectively,

$$\begin{aligned} \mathbf{S}_{\mathbf{r},n}^{\,2} &= S^2 \\ \sum_{\mathbf{k},\mathbf{k'}} e^{i(\mathbf{k}+\mathbf{k'})\cdot\mathbf{r}}\ \mathbf{S}_{\mathbf{k},n}\cdot\ \mathbf{S}_{\mathbf{k'},n} &= S^2, \forall \mathbf{r}. \end{aligned} \tag{3.1.1}$$

The LT method, on the other hand, replaces this constraint with a weaker constraint [16, 22, 23], which is

$$\begin{aligned} \sum_{\mathbf{r},n} \mathbf{S}_{\mathbf{r},n}^{\,2} &= 3N_{u.c.}S^2 \\ \sum_{\mathbf{k},n} \mathbf{S}_{\mathbf{k},n}\cdot\ \mathbf{S}_{\mathbf{-k},n} &= 3S^2. \end{aligned} \tag{3.1.2}$$

Where $\mathbf{r}$ denotes the position of unit cell, and $n = 1, 2, 3$ denotes the sublattice index.

Observe that if we had to use the equation with the strong constraint, we would need to solve N non-linear equations simultaneously. However, with the help of the LT method, we only need to solve single constraint equation which is linear. By applying LT method, we assume that local fields on all sites are the same. If the solution to the LT problem happens to satisfy the strong constraints as well, then we have also solved the original, much harder, problem.

In order to use the LT method to minimize the energy, we first need to use the method of Lagrange multipliers by using the weak constraint,

$$\begin{aligned} F &= \epsilon - \lambda \left(\sum_{\mathbf{k},n} \mathbf{S}_{\mathbf{k},n} \cdot \mathbf{S}_{-\mathbf{k},n} - 3S^2 \right) \\ \frac{\partial F}{\partial S^{\gamma}_{-\mathbf{k},n}} &= 0 \quad \rightarrow \quad \sum_{m=1,2,3} \Lambda^{\gamma}_{nm} S_{\mathbf{k},m} = \lambda S^{\gamma}_{\mathbf{k},n}. \end{aligned} \tag{3.1.3}$$

Where $\epsilon = H/N_{u.c.}$, $\gamma = x, y, z$ is the bond index, and $m = 1, 2, 3$ is the sublattice index.

Meaning, different bond indices, γ, decouple from each other and, so, we only need to diagonalize 3×3 $\Lambda^x, \Lambda^y, \Lambda^z$ matrices. Lets assume that we can satisfy these relations with a single Lagrange multiplier, λ, then, we can re-express the energy in the following;

$$\begin{aligned} H/N_{u.c.} &= \sum_{\mathbf{k},\gamma,n} S^{\gamma}_{-\mathbf{k},n} \sum_{m} \Lambda^{\gamma}_{n,m}(\mathbf{k}) S^{\gamma}_{\mathbf{k},m} \\ &= \lambda \sum_{\mathbf{k},n} \mathbf{S}_{\mathbf{k},n} \dot{\mathbf{S}}_{-\mathbf{k},n} \rightarrow H/N_{u.c.} = 3\lambda S^2. \end{aligned} \tag{3.1.4}$$

This means we can minimize the energy by minimizing the eigenvalue λ over the 1st BZ.

3.2 Luttinger-Tizsa method for Kitaev-Heisenberg model

Lets first write an explicit form for the Hamiltonian, (2.1.1), in the momentum space using the Fourier transformation:

$$\begin{aligned}
\hat{H} &= J\sum_{\mathbf{k}}[(\ \mathbf{S}_{\ \mathbf{k},1}\cdot\ \mathbf{S}_{\ -\mathbf{k},2}+\ \mathbf{S}_{\ \mathbf{k},1}\cdot\ \mathbf{S}_{\ -\mathbf{k},3}+\mathbf{S}_{\ \mathbf{k},2}\cdot\ \mathbf{S}_{\ -\mathbf{k},3}) \\
&+ (\ \mathbf{S}_{\mathbf{k},1}\cdot\ \mathbf{S}_{\ -\mathbf{k},2}e^{i\frac{\mathbf{k}_x}{2}}+\ \mathbf{S}_{\ \mathbf{k},1}\cdot\ \mathbf{S}_{\ -\mathbf{k},3}e^{i(\frac{k_x+\sqrt{3}k_y}{4})}+\mathbf{S}_{\ \mathbf{k},2}\cdot\ \mathbf{S}_{\ -\mathbf{k},3}e^{i(\frac{-k_x+\sqrt{3}k_y}{4})})] \\
&+ K\sum_{\mathbf{k}}[(S^x_{\mathbf{k},2}S^x_{-\mathbf{k},3}+S^x_{\mathbf{k},2}S^x_{-\mathbf{k},3}e^{i(\frac{-k_x+\sqrt{3}k_y}{4})}+(S^y_{\mathbf{k},1}S^y_{-\mathbf{k},3}+S^y_{\mathbf{k},1}S^y_{\ -\mathbf{k},3}e^{i(\frac{k_x+\sqrt{3}k_y}{4})}) \\
&+ (S^z_{\mathbf{k},1}S^z_{-\mathbf{k},2}+S^z_{\mathbf{k},1}S^z_{-\mathbf{k},3}e^{i\frac{k_x}{2}})].
\end{aligned} \tag{3.2.1}$$

We can put this in more compact form as

$$\hat{H}=\sum_{\mathbf{k},\alpha,n,m}S^{\alpha}_{\mathbf{k},n}\Lambda^{\alpha}_{n,m}\left(\mathbf{k}\right)S^{\alpha}_{-\mathbf{k},m}.$$

Where the matrix Λ is a 3 by 3 matrix for each x,y,z axes, and can be represented as

$$\Lambda=\begin{pmatrix}\Lambda^x & 0 & 0\\ 0 & \Lambda^y & 0\\ 0 & 0 & \Lambda^z\end{pmatrix}. \tag{3.2.2}$$

$$\begin{aligned}
\Lambda^x_{11} &= \Lambda^x_{22}=\Lambda^x_{33}=0 \\
\Lambda^x_{12} &= \frac{J}{2}\left(1+e^{ik_x}\right),\quad \Lambda^x_{21}=(\Lambda^x_{12})^* \\
\Lambda^x_{13} &= \frac{J}{2}\left(1+e^{i\left(\frac{k_x}{2}+\frac{\sqrt{3}k_y}{2}\right)}\right),\quad \Lambda^x_{31}=(\Lambda^x_{13})^* \\
\Lambda^x_{23} &= \frac{(J+K)}{2}\left(1+e^{i\left(\frac{-k_x}{2}+\frac{\sqrt{3}k_y}{2}\right)}\right),\quad \Lambda^x_{32}=(\Lambda^x_{23})^*.
\end{aligned} \tag{3.2.3}$$

$$\begin{aligned}
\Lambda^y_{11} &= \Lambda^y_{22} = \Lambda^y_{33} = 0 \\
\Lambda^y_{12} &= \frac{J}{2}\left(1 + e^{ik_x}\right), \quad \Lambda^y_{21} = \left(\Lambda^y_{12}\right)^* \\
\Lambda^y_{13} &= \frac{(J+K)}{2}\left(1 + e^{i\left(\frac{k_x}{2} + \frac{\sqrt{3}k_y}{2}\right)}\right), \quad \Lambda^y_{31} = \left(\Lambda^y_{13}\right)^* \\
\Lambda^y_{23} &= \frac{J}{2}\left(1 + e^{i\left(\frac{-k_x}{2} + \frac{\sqrt{3}k_y}{2}\right)}\right), \quad \Lambda^y_{32} = \left(\Lambda^y_{23}\right)^*.
\end{aligned} \tag{3.2.4}$$

$$\begin{aligned}
\Lambda^z_{11} &= \Lambda^z_{22} = \Lambda^z_{33} = 0 \\
\Lambda^z_{12} &= \frac{(J+K)}{2}\left(1 + e^{ik_x}\right), \quad \Lambda^z_{21} = \left(\Lambda^z_{12}\right)^* \\
\Lambda^z_{13} &= \frac{J}{2}\left(1 + e^{i\left(\frac{k_x}{2} + \frac{\sqrt{3}k_y}{2}\right)}\right), \quad \Lambda^z_{31} = \left(\Lambda^z_{13}\right)^* \\
\Lambda^y_{23} &= \frac{J}{2}\left(1 + e^{i\left(\frac{-k_x}{2} + \frac{\sqrt{3}k_y}{2}\right)}\right), \quad \Lambda^z_{32} = \left(\Lambda^z_{23}\right)^*.
\end{aligned} \tag{3.2.5}$$

All Λ matrices are symmetric and Hermitian, so, once we write down the characteristic equation, we can realize that the existent polynomial is nothing but a depressed cubic equation.

3.3 Analytical solution for the ground state of Kitaev-Heisenberg model

In this section we will find an analytical solution to the minimum energy configuration for the KH model. See that characteristic equations for each Λ-matrices are nothing but the depressed cubic equations.

Since all Λ-matrices are identical, i.e. can be transformed to each other by $2\pi/3$ rotations, we can choose one of the Λ-matrices and work on it. Other Λ-matrices will follow the same calculation scheme. So, let's choose Λ^x.

First, re-define (3.2.5) as

$$\Lambda^x = \begin{pmatrix} 0 & a & b \\ a* & 0 & c \\ b* & c* & 0 \end{pmatrix}. \tag{3.3.1}$$

where we take

$$\begin{aligned} a &= 2Je^{i\frac{k_x}{2}} \cos\left(\frac{k_x}{2}\right) \\ b &= 2Je^{i(\frac{k_x+\sqrt{3}k_y}{4})} \cos\left(\frac{k_x+\sqrt{3}k_y}{4}\right) \\ c &= 2(J+K)e^{i(\frac{-k_x+\sqrt{3}k_y}{4})} \cos\left(\frac{-k_x+\sqrt{3}k_y}{4}\right). \end{aligned} \tag{3.3.2}$$

So, the characteristic equation comes with taking the determinant $det\,(\Lambda^x - \lambda I) = 0$

$$\lambda^3 - \left(|a|^2 + |b|^2 + |c|^2\right)\lambda - (acb^* + a^*c^*b) = 0. \tag{3.3.3}$$

Where we define [15]

$$
\begin{aligned}
p &= -\left(|a|^2+|b|^2+|c|^2\right) \\
p &= -[4(j+k)^2\cos^2\left(\frac{k_x-\sqrt{3}k_y}{4}\right)+4j^2[\cos^2\left(\frac{k_x+\sqrt{3}k_y}{4}\right)+\cos^2\left(\frac{k_x}{2}\right)]] \\
q &= -\left(acb^*+a^*c^*b\right) \\
q &= -[8j^2(j+k)\cos\left(\frac{k_x}{2}\right)\cos\left(\frac{k_x+\sqrt{3}k_y}{4}\right)\cos\left(\frac{k_x-\sqrt{3}k_y}{4}\right)].
\end{aligned}
\tag{3.3.4}
$$

So, we can write the analyical form of the eigenvalues as

$$
\begin{aligned}
\varphi &= \cos^{-1}\left(-\frac{q}{2\left(-\frac{p}{3}\right)^{3/2}}\right) \\
\lambda_1 &= 2\sqrt{-\frac{p}{3}}\cos\left(\frac{\varphi}{3}\right) \\
\lambda_2 &= -\sqrt{-\frac{p}{3}}\left(\sqrt{3}\sin\left(\frac{\varphi}{3}\right)+\cos\left(\frac{\varphi}{3}\right)\right) \\
\lambda_3 &= -\sqrt{-\frac{p}{3}}\left(\cos\left(\frac{\varphi}{3}\right)-\sqrt{3}\sin\left(\frac{\varphi}{3}\right)\right).
\end{aligned}
\tag{3.3.5}
$$

with p, q are given in (3.3.4).

3.4 Special characteristic solutions at the Kitaev limit

In this section, we will work on the calculation of the ordering vectors, namely Q-vectors, for the Kitaev limit. Then, we will calculate the GS energy for this specific limit by using the Q-vectors we have found and further discuss the degeneracy of the GS.

It's an intuitive approach to show how we can find the solutions of KH model that match with the results obtained from LT method.

3.4.1 Ordering vector calculation for a specific configuration of one of the ground states for Kitaev limit

In this section, we will work on the Kitaev limit over different bonds. We will see that all Q-vectors which are found from each specific configuration will give the minimum

energy configuration that would match with the LT method.

3.4.1.1 Q-Vector for zz-bond, K>0, J=0

For simplicity, we only show one of the sublattices and we draw the triangular Bravais lattice.

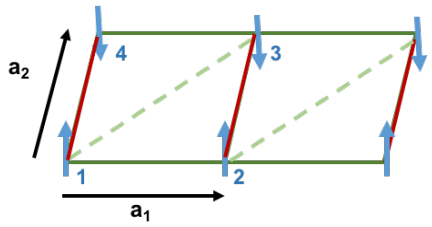

Figure 3.1: Spins are anti-ferrogamnetically placed over zz bonds (colored as green) with primitive lattice vectors $\mathbf{a}_1$ and $\mathbf{a}_2$. Dashed lines indicate the unit cell (u.c.).

We can represent an up spin and a down spin in vectorial form, respectively, as

$$\begin{aligned} \mathbf{S}_{\uparrow}(\mathbf{r}) &= e^{i\,\mathbf{Q}\cdot\mathbf{r}}\,\mathbf{S}_0 \\ \mathbf{S}_{\downarrow}(\mathbf{r}) &= e^{i\,\mathbf{Q}\cdot\mathbf{r}}\,(-\mathbf{S}_0)\,. \end{aligned} \tag{3.4.1}$$

Where $|\mathbf{S}_0|^2 = 1$ and $\mathbf{S}_0 = \hat{z}$.

In order to calculate the Q-vector for a specific configuration we can use Eq. (3.4.1) both with the same spin orientation, i.e. up-up or down-down, and with the opposite spin orientation, i.e. up-down or down-up.

So, for $\mathbf{r}_1 = (0,0)\,,\quad \mathbf{r}_2 = (1,0)\,,\quad \mathbf{r}_4 = \left(\frac{1}{2}, \frac{\sqrt{3}}{2}\right)$, where r is the position of sublattices within the u.c.

$$\begin{aligned} \mathbf{S}_{\uparrow}(0,0) &= e^{i\,\mathbf{Q}\cdot(0,0)}\mathbf{S}_{\,0} = \mathbf{S}_{\,0} \\ \mathbf{S}_{\uparrow}(1,0) &= e^{i\,\mathbf{Q}\cdot(1,0)}\,\mathbf{S}_{\,0} = \mathbf{S}_{\,0} \\ \mathbf{S}_{\downarrow}\left(\frac{1}{2},\frac{\sqrt{3}}{2}\right) &= e^{i\,\mathbf{Q}\cdot\left(\frac{1}{2},\frac{\sqrt{3}}{2}\right)}\,\mathbf{S}_{\,0} = -\mathbf{S}_{\,0}. \end{aligned} \tag{3.4.2}$$

Solving Eq. (3.4.2) for $\mathbf{Q}$ gives

$$\mathbf{Q}_z = \left(0, \frac{2\pi}{\sqrt{3}}\right). \tag{3.4.3}$$

We see that $\mathbf{Q}_z$ is positioned exactly at the same location as one of the high-symmetry points,$\mathbf{M}_z$, on the 1st BZ.

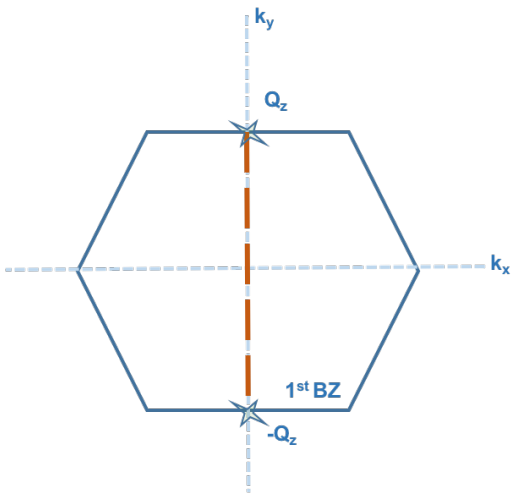

Figure 3.2: 1st BZ of the kagome lattice with zz bond and the corresponding Q-vector solution emphasized.

3.4.1.2 Ground state energy per unit cell for zz-bond, K>0, J=0

GS energy for such a configuration is

$$E^{zz} = K \sum_{\mathbf{r}} (S^z_{\mathbf{r},1} S^z_{\mathbf{r},2} + S^z_{\mathbf{r}+\mathbf{a}_2,1} S^z_{\mathbf{r}+\mathbf{a}_2-\mathbf{a}_1,2}). \tag{3.4.4}$$

With $\mathbf{Q}_z = (0, \frac{2\pi}{\sqrt{3}})$ and position vectors,

$$\begin{aligned} \mathbf{r},1 &= \mathbf{r},2 = (0,0) \\ \mathbf{r}+\mathbf{a}_2,1 &= (\frac{1}{2}, \frac{\sqrt{3}}{2}) \\ \mathbf{r}+\mathbf{a}_2-\mathbf{a}_1,2 &= (-\frac{1}{2}, \frac{\sqrt{3}}{2}). \end{aligned} \tag{3.4.5}$$

Note that $\mathbf{a}_1 = (1,0)$ and $\mathbf{a}_2 = (\frac{1}{2}, \frac{\sqrt{3}}{2})$.

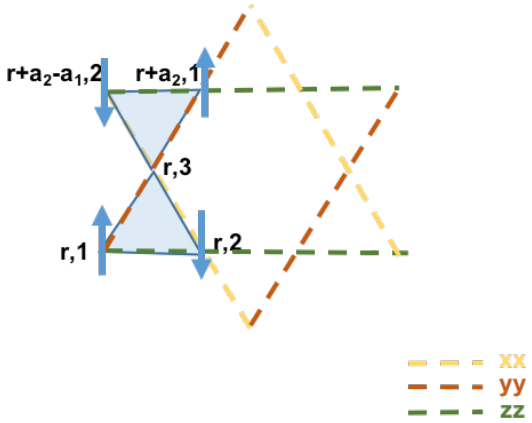

Figure 3.3: Spins are anti-ferrogamnetically placed over zz bonds. Shaded triangles represents u.c. states.

Observe that we drop the first and second terms in the Hamiltonian in (3.2.1) because spins are along z-direction and their map on x,y-directions is zero. So we don't have any contributions to the Hamiltonian from those terms.

We can represent the real space spin vectors as

$$\begin{aligned} \mathbf{S}_{\uparrow}(\ \mathbf{r}\ ) &= e^{i\ \mathbf{Q}\ \cdot\ \mathbf{r}}\ \mathbf{S}_0 \\ \mathbf{S}_{\downarrow}(\ \mathbf{r}\ ) &= e^{i\ \mathbf{Q}\ \cdot\ \mathbf{r}}\ (-\mathbf{S}_{\ 0})\,. \end{aligned} \tag{3.4.6}$$

Substituting (3.4.5) and (3.4.6) into (3.4.4) will give energy per unit cell states (u.c.s.),

$$\begin{aligned} \epsilon^{zz} &= \frac{E^{zz}}{N_{u.c.s.}} = K[e^{i\mathbf{Q}^{zz}.(0,0)}\ \mathbf{S}_{\ 0} e^{i\mathbf{Q}^{zz}.(0,0)}\,(-\ \mathbf{S}_{\ 0}) + e^{i\mathbf{Q}^{zz}.(\frac{1}{2},\frac{\sqrt{3}}{2})}\,(-\mathbf{S}_{\ 0})\,e^{i\mathbf{Q}^{zz}.(-\frac{1}{2},\frac{\sqrt{3}}{2})}\mathbf{S}_{\ 0}] \\ &= -2K. \end{aligned} \tag{3.4.7}$$

Note that $|\mathbf{S}_0|^2 = 1$. Since in this case $N_{u.c.s.} = N_{u.c.}$, we simply have $\epsilon^{zz} = -2K$.

3.4.1.3 Q-Vector for yy-bond, K>0, J=0

For the yy-bond, we can again choose one of the sublattices which has AFM order on this bond. Meaning, Fig.2.4 has an equivalent form to Fig.2.5, as one can see below,

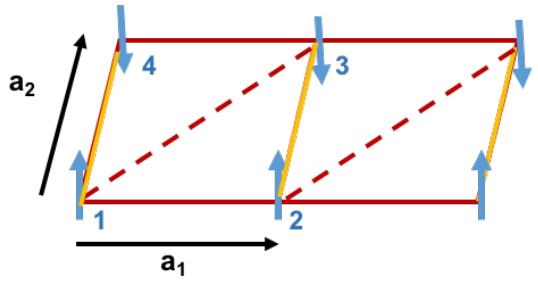

Figure 3.4: Spins are anti-ferrogamnetically placed over yy bonds (colored as red) with primitive lattice vectors $\mathbf{a}_1$ and $\mathbf{a}_2$. Dashed lines indicate the unit cell (u.c.).

We can again represent the spin vectors as in Eq. (3.4.1), and calculate the Q-vector henceforth.

Note that, the position vectors now become $\mathbf{r}_1 = (0,0)\,, \mathbf{r}_2 = \left(\frac{1}{2}, \frac{\sqrt{3}}{2}\right), \mathbf{r}_4 = (1,0)\,.$

$$\begin{aligned}
\mathbf{S}_{\uparrow}(\mathbf{r}_1) &= e^{i\,\mathbf{Q}\cdot\mathbf{r}_1}\,\mathbf{S}_0 = \mathbf{S}_0 \\
\mathbf{S}_{\uparrow}(\mathbf{r}_2) &= e^{i\,\mathbf{Q}\cdot\mathbf{r}_2}\,\mathbf{S}_0 = \mathbf{S}_0 \\
\mathbf{S}_{\downarrow}(\mathbf{r}_4) &= e^{i\,\mathbf{Q}\cdot\mathbf{r}_4}\,\mathbf{S}_0 = -\,\mathbf{S}_0.
\end{aligned} \tag{3.4.8}$$

We now have and $\mathbf{S}_0 = \hat{y}$. Solving Eq. (3.4.8) for $\mathbf{Q}$ will lead a result

$$\mathbf{Q}_y = \left(-\pi, \frac{\pi}{\sqrt{3}}\right). \tag{3.4.9}$$

We see that $\mathbf{Q}_y$ is positioned exactly at the same location as one of the high-symmetry points,$\mathbf{M}_y$, on the 1st BZ.

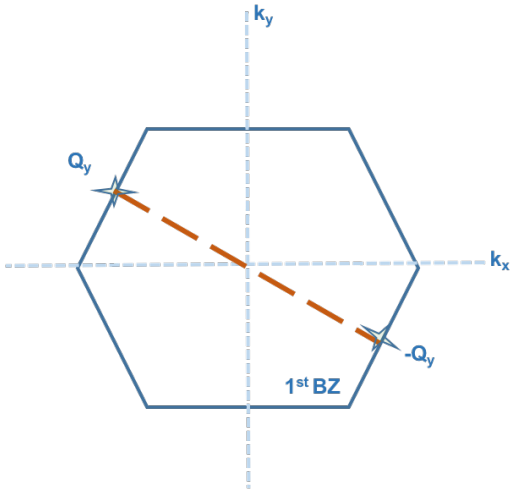

Figure 3.5: 1st BZ of the kagome lattice with yy bond and the corresponding Q-vector solution emphasized.

3.4.1.4 Ground state energy per unit cell for yy-bond, K>0, J=0

GS energy for such a configuration is

$$E^{yy} = K\sum_{\mathbf{r}}(S^y_{\mathbf{r},1}S^y_{\mathbf{r},3} + S^y_{\mathbf{r}+\mathbf{a}_1,1}S^y_{\mathbf{r}-(\mathbf{a}_2-\mathbf{a}_1),3}). \tag{3.4.10}$$

With Q-vector $\mathbf{Q}_y = (-\pi, \frac{\pi}{\sqrt{3}})$.

Observe that we drop the first and third terms in the Hamiltonian, (3.2.1), because spins are along y-direction.

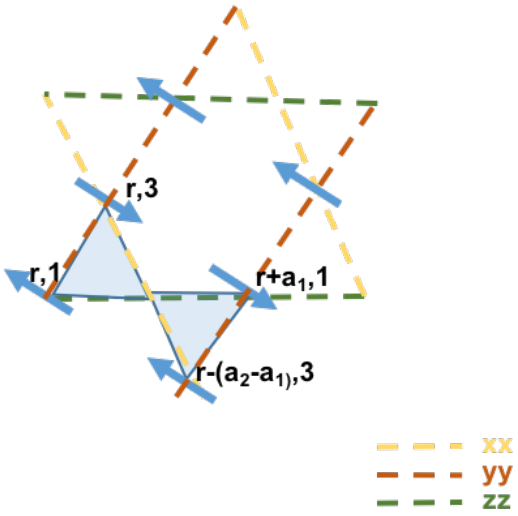

Figure 3.6: Spins are anti-ferrogamnetically placed over yy bonds. Shaded triangles represent u.c. states.

Following a similar substitution process as in Sec. 3.4.1.2 will give energy per u.c.s. as

$$\begin{aligned} \epsilon^{yy} &= \frac{E^{yy}}{N_{u.c.s.}} = K[e^{i\mathbf{Q}^{yy}.(\frac{1}{2},-\frac{\sqrt{3}}{2})}\ \mathbf{S}_{\ 0} e^{i\mathbf{Q}^{yy}}.(1,0)\,(-\ \mathbf{S}_{\ 0}) + e^{i\mathbf{Q}^{yy}.(0,0)}\ \mathbf{S}_{\ 0} e^{i\mathbf{Q}^{yy}.(0,0)}\,(-\ \mathbf{S}_{\ 0})] \\ &= -2K. \end{aligned} \tag{3.4.11}$$

Since in this case $N_{u.c.s.} = N_{u.c.}$, we simply have $\epsilon^{yy} = -2K$.

3.4.1.5 Q-Vector for xx-bond, K>0, J=0

For the xx-bond, we can again choose one of the sublattices which has AFM order on this bond. Meaning, Fig.3.6 has an equivalent form to Fig.3.7, as one can see below,

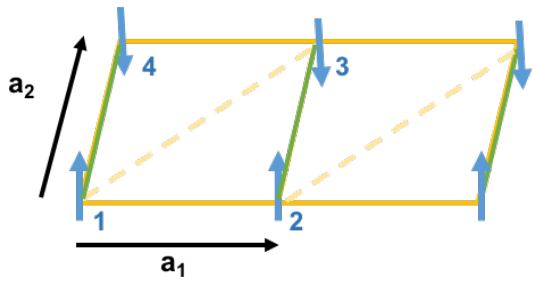

Figure 3.7: Spins are anti-ferrogamnetically placed over xx bonds (colored as yellow) with primitive lattice vectors $\mathbf{a}_1$ and $\mathbf{a}_2$. Dashed lines indicate the unit cell (u.c.).

We can again represent the spin vectors as in Eq. (3.4.1), and calculate the Q-vector henceforth.

Note that, the position vectors now become $\mathbf{r}_1 = (0,0)\,, \mathbf{r}_2 = \left(-\frac{1}{2}, \frac{\sqrt{3}}{2}\right), \mathbf{r}_4 = (1,0)$.

$$\begin{aligned} \mathbf{S}_{\uparrow}(\mathbf{r}_1) &= e^{i\,\mathbf{Q}\cdot\mathbf{r}_1}\,\mathbf{S}_0 = \mathbf{S}_0 \\ \mathbf{S}_{\uparrow}(\mathbf{r}_2) &= e^{i\,\mathbf{Q}\cdot\mathbf{r}_2}\,\mathbf{S}_0 = \mathbf{S}_0 \\ \mathbf{S}_{\downarrow}(\mathbf{r}_4) &= e^{i\,\mathbf{Q}\cdot\mathbf{r}_4}\,\mathbf{S}_0 = -\,\mathbf{S}_0. \end{aligned} \tag{3.4.12}$$

For this case, we have and $\mathbf{S}_0 = \hat{x}$. Solving Eq. (3.4.12) for $\mathbf{Q}$ will lead a result

$$\mathbf{Q}_x = \left(\pi, \frac{\pi}{\sqrt{3}}\right). \tag{3.4.13}$$

To illustrate this better, we see that $\mathbf{Q}_x$ is positioned exactly at the same location as one of the high-symmetry points,$\mathbf{M}_x$, on the BZ.

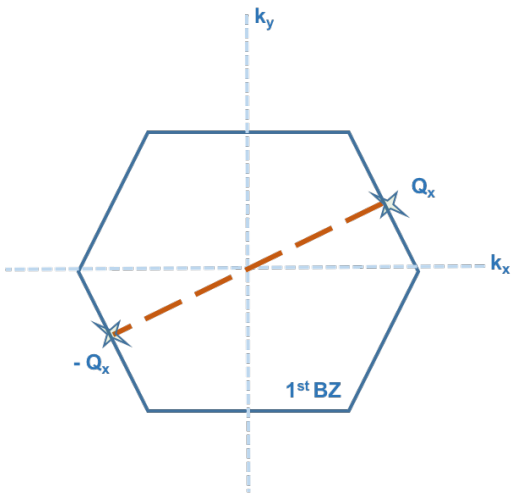

Figure 3.8: BZ of the kagome lattice with xx bond and the corresponding Q-vector solution emphasized.

3.4.1.6 Ground state energy per unit cell for xx-bond, K>0, J=0

GS energy for such a configuration is

$$E^{xx} = K \sum_{\mathbf{r}} (S^x_{\mathbf{r}-\mathbf{a}_1,2} S^x_{\mathbf{r}-\mathbf{a}_2,3} + S^x_{\mathbf{r},2} S^x_{\mathbf{r},3}) \tag{3.4.14}$$

With Q-vector $\mathbf{Q}_x = (-\pi, -\frac{\pi}{\sqrt{3}})$.

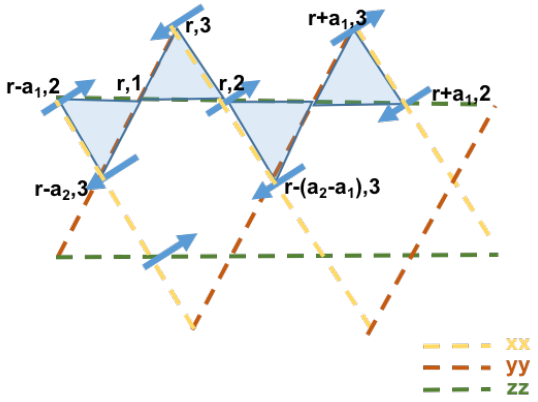

Figure 3.9: Spins are anti-ferrogamnetically placed over xx bonds. Shaded triangles represent u.c. states.

Observe that we drop the second and third terms in the Hamiltonian, (3.2.1), because spins are along x-direction.

Following a similar substitution process as in Sec. 3.4.1.2 will give $\frac{E^{xx}}{N_{u.c.s.}} = -2K$. Since in this case $N_{u.c.s.} = N_{u.c.}$, we simply have $\epsilon^{xx} = -2K$.

In this section, we observed with simple illustrative examples of "sliding symmetry". The sliding symmetry involves flipping the spins simultaneously along a single row or column of the lattice [**?**] . These discrete symmetry transformations stand in-between the global symmetries and the local symmetries of gauge theories. In terms of the LT approach, this sliding symmetry means that any Q-point from the line of the minimum eigenvalues gives a GS solution.

As to the degeneracy for Kitaev limit, we can calculate it as follows. Let's define $N \equiv$ number of lattice sites, $N_{d.s.} \equiv$ number of dangling sites, $N_\gamma \equiv$ number of γ lines, where $\gamma = \{xx, yy, zz\}$. Note that $N_{xx} = N_{yy} = N_{zz}$. So, the total number of degenerate ground states is then,

$$d_{TOT} = 3 \times 2^{N_{d.s.}} \times 2^{N_\gamma}. \tag{3.4.15}$$

Where $N_{d.s.} = N/3$ and $N_\gamma = \sqrt{N/3}$, with $N = 3 \times N_{u.c.}$. So, because of the dangling spins the degeneracy is extensive, i.e. it grows exponentially with the system

size.

The LT results show that for the Kitaev limit any point on the line of Γ - Q_i where $i = \{x, y, z\}$ is a solution for the eigenvalue equation.

To illustrate this better, one can take a look at the eigenenergy solutions for xx, yy, and zz bonds ,respectively, in below figures

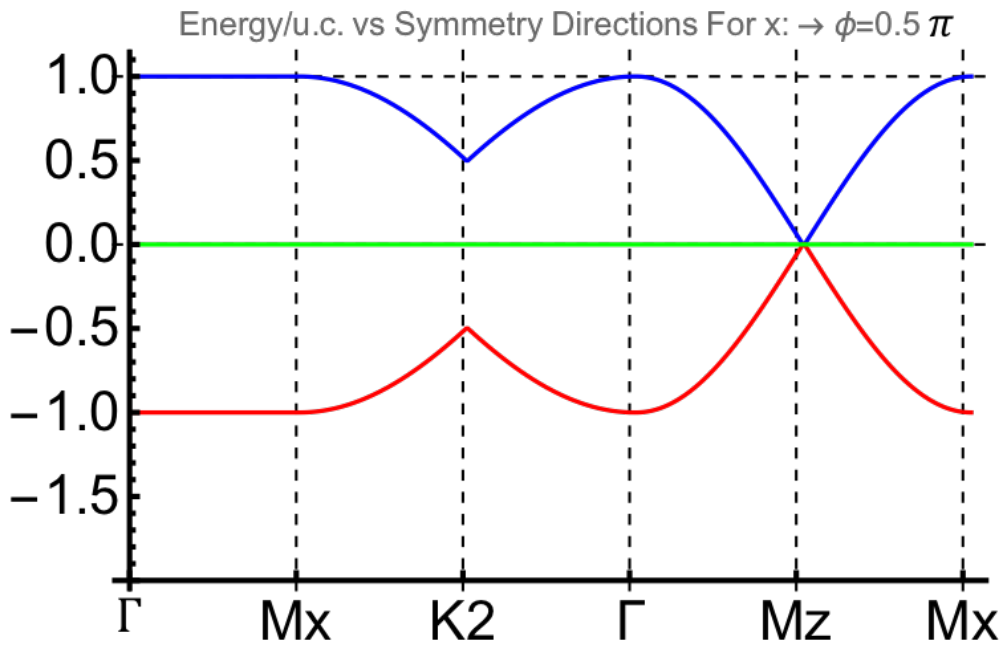

Figure 3.10: Eigenenergy solution for Kitaev limit at $\phi = 0.5\pi$ for Λ^x obtained with the LT method. Three different colors indicates three eigenvalues obtained from Λ^x matrix.

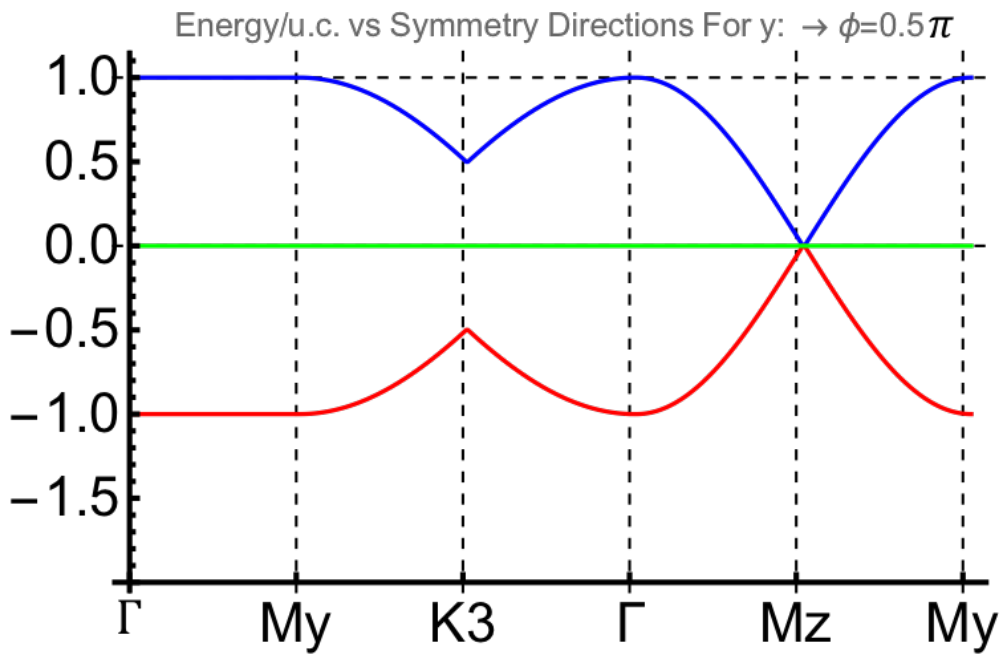

Figure 3.11: Eigenenergy solution for Kitaev limit at $\phi = 0.5\pi$ for Λ^y obtained with the LT method.Three different colors indicates three eigenvalues obtained from Λ^y matrix.

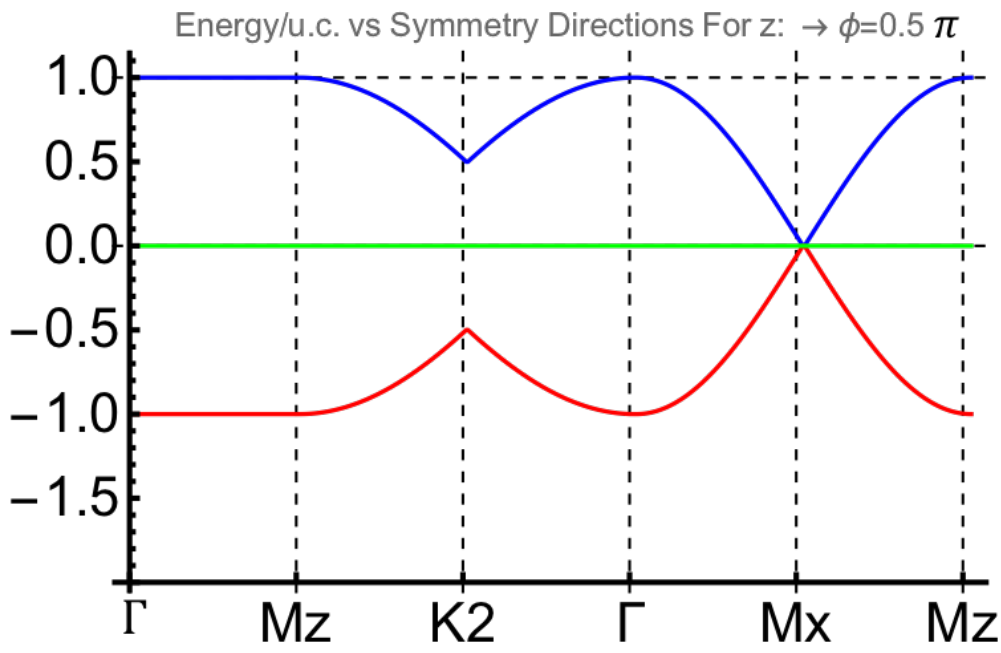

Figure 3.12: Eigenenergy solution for Kitaev limit at $\phi = 0.5\pi$ for Λ^z obtained with the LT method.Three different colors indicates three eigenvalues obtained from Λ^z matrix.

Figures, Fig.3.10-3.12, show the minimum energy solutions (on the left of each figure) of Λ^x, Λ^y, and Λ^z matrices respectively which we obtained by the LT method. See that GS energy solution corresponds to a line on the 1st BZ (on the right of each figure) of the kagome lattice for each Λ matrices.

3.4.2 Ground state energy per unit cell for AFM Heisenberg limit, K=0 and J>0

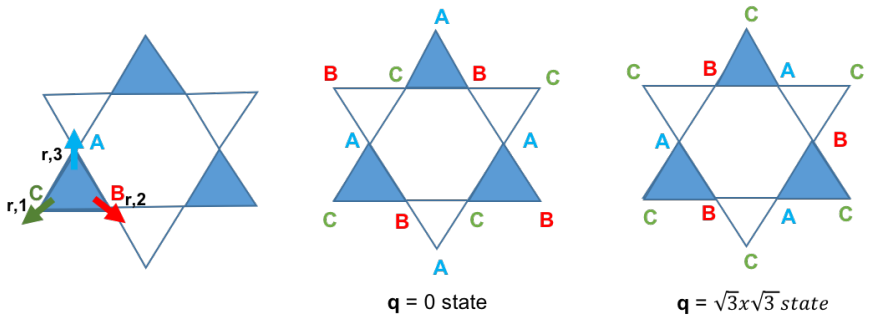

Figure 3.13: Left, 3-sublattice spin orientation on kagome lattice; Middle, $\mathbf{q} = 0$ state configuration for AFMH; Right, $\mathbf{q} = \sqrt{3}x\sqrt{3}$ state configuration for AFMH.

In this section, we will work on the ground state energy per u.c. for AFMH limit, i.e. $K = 0$ and $J > 0$, and compare it with the LT result. In Fig.3.13, here, we give two of the infinitely many GS configurations of AFMH as an illustrative example. Classical ground state configurations can be obtained by minimizing the exchange energy, see Chapter-1, for each triangle. All the pseudo-spin vectors lie along the angle bisectors of each triangle, which can be arranged such that 120^o state over the whole lattice is obtained. This idea was first suggested by Baxter in his paper [3]. Similarly, we use the color labeling in Fig. 3.13 to show degenerate GS configurations. In this limit can be written as following

$$\begin{aligned} \hat{H}_H &= J \sum_{<i,j>} \mathbf{S}_i \cdot \mathbf{S}_j \\ &= \frac{J}{2} \sum_{\alpha} (\mathbf{S}_A + \mathbf{S}_B + \mathbf{S}_C)^2 - \frac{J}{2} \sum_{\alpha} (\mathbf{S}_A^2 + \mathbf{S}_B^2 + \mathbf{S}_C^2) \end{aligned} \tag{3.4.16}$$

Where α defines the total number of triangles, which is equal to $\frac{2N}{3}$, and N is the total number of sites. In order to have a GS in the AFMH limit, total spin vector in

each triangle must add up to zero. So, first term in (3.4.16) drops out. Since we have $|\mathbf{S}|^2 = 1$, second term would just bring factor of 3 under the summation sign, i.e. it gives the constant energy contribution. Note that we need energy per u.c. and $N_{u.c.} = \frac{N}{3}$. If we plug this number into (3.4.16), then we would obtain $\hat{H}_H = -3J$. So, the result we found here matches with the result obtained in LT method for the Heisenberg limit.

Observe that all the GS configurations is a replica of \or $\mathbf{q} = 0$ state. Changing between these two states doesn't cost any energy.

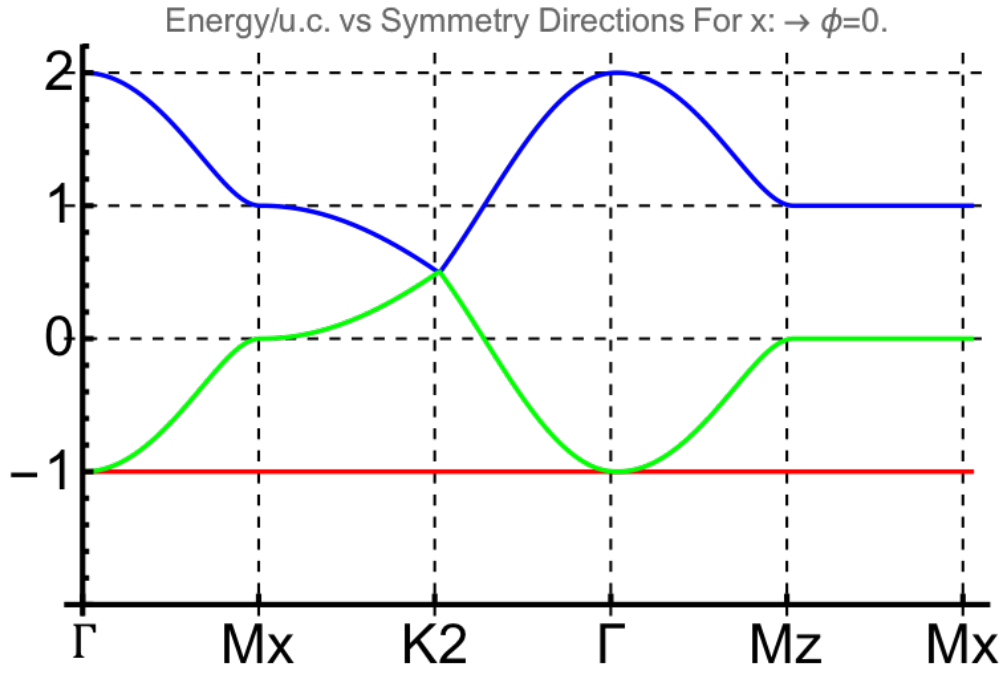

Figure 3.14: Eigenenergy solution for Heisenberg limit at $\phi = 0$ which is obtained from the LT method. Three different colors indicate three eigenvalues obtained from Λ^x matrix.

As one can see in Fig. 3.14, in AFM Heisenberg limit, minimum energy corresponds to a flat band which is colored by a red line. This means that any q-vector on the 1st BZ satisfies the GS energy solution, and correspondingly, the minimum energy solution contains infinitely many configurations, i.e. colinear, non-colinear, coplanar, and non-coplanar states [24, 27, 30].

Chapter 4

Three Sublatice Transformation

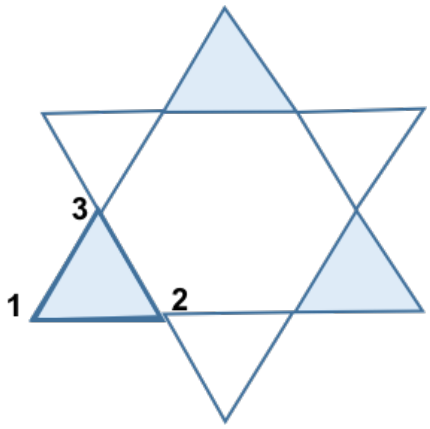

Figure 4.1: Kagome lattice divided into 3 sublattices where 1-3 represent sublattice indices.

On the phase diagram, in Fig.1.4, we can see well-known isolated points; a,b,d, and e. However, there are more isolated points entering the phase diagram that were hidden at the first glance. These points correspond to some random points on the phase diagram in unrotated frame; however, after we do π-rotation about x and y axes at all sites belonging to the sublattices 1 and 2, we see that these random points actually map to well known isolated points in rotated frame. In order to detect them, we use a special technique that is known as four-sublattice transformation which was originally

introduced for the KH model on the honeycomb lattice [14,21]; here, we need to modify it to make it applicable for the kagome lattice.

The model we have has a duality transformation that amounts to rotating the spins of each of the three sublattices to different local reference frames, as follows:

$$\begin{aligned}
\tilde{\mathbf{S}}_{\mathbf{r},1} &= \left(-S^x_{\mathbf{r},1}, S^y_{\mathbf{r},1}, -S^z_{\mathbf{r},1}\right) \\
\tilde{\mathbf{S}}_{\mathbf{r},2} &= \left(S^x_{\mathbf{r},2}, -S^y_{\mathbf{r},2}, -S^z_{\mathbf{r},2}\right) \\
\tilde{\mathbf{S}}_{\mathbf{r},3} &= \left(S^x_{\mathbf{r},3}, S^y_{\mathbf{r},3}, S^z_{\mathbf{r},3}\right), \forall \mathbf{r}
\end{aligned} \tag{4.0.1}$$

Where 1,2,3 refers to the spins lying in three sublattices respectively.

With the help of Fig.4.1 above, we can write the new, transformed, Hamiltonian as

$$\begin{aligned}
\tilde{H} &= \tilde{J} \sum_{<i,j>} \tilde{\mathbf{S}}_i \cdot \tilde{\mathbf{S}}_j + \tilde{K} \sum_{<i,j>} S_i^{\tilde{\gamma}_{ij}} S_j^{\tilde{\gamma}_{ij}} \\
\hat{H} &= -J \sum_{<i,j>} \mathbf{S}_i \cdot \mathbf{S}_j + (K + 2J) \sum_{<i,j>} S_i^{\gamma_{ij}} S_j^{\gamma_{ij}}
\end{aligned} \tag{4.0.2}$$

Where $< i, j >$ is the n.n. lattice vectors, γ is the bond direction. Observe that the transformed Hamiltonian has exactly the same form as the original Hamiltonian except for the change in coupling constants. So, new coupling constants together with the mapped parametrization angle now becomes

$$\begin{aligned}
\tilde{J} &= -J \\
\tilde{K} &= K + 2J \\
tan(\tilde{\phi}) &= -tan(\phi) - 2
\end{aligned} \tag{4.0.3}$$

Where $\phi \epsilon [0, 2\pi]$ is parametrization angle. We see immediately that when $\tilde{K} = K + 2J = 0$ we get an isotropic SO(3) Heisenberg model in the rotated frame. Specifically,

for $\phi = arctan(-2)$ we get $\tilde{K} = 0$ and $\tilde{J} = -1$, i.e. a FM Heisenberg model, while for $\phi = arctan(-2) + \pi$ we get $\tilde{K} = 0$ and $\tilde{J} = 1$, i.e. a AF Heisenberg model. These two points define our dual SO(3) symmetric points of the model that we mentioned earlier.

By using the mapped parametrization angle, we can also map different regions of the phase diagram to each other, as follows; region (1) of Fig.1.4 maps to itself, region (2) maps to (4), region (3) maps to (5). Similarly, the isolated point HAFM maps to its dual-HAFM, HFM maps to its dual-HFM, and the Kitaev points are self-dual.

Chapter 5

Results

In this chapter, we will discuss the eigenvectors obtained with LT method and comment on the states on the classical phase diagram.

5.0.1 Eigenvectors for Kitaev limit

1. $\Lambda^z(k)$ Matrix:

   As it is indicated with the LT method, minimum energy solution for zz-bond is given as any point on the line $\mathbf{M}_z - \Gamma$ in BZ. See Fig.5.1 below.

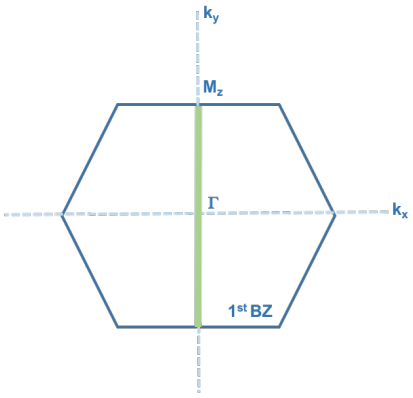

Figure 5.1: Minimum energy line on zz bond over the 1st BZ indicated.

For $\mathbf{k} = \mathbf{M}_z$, the minimum eigenvalue, λ_{min} corresponds to the eigenvector,

$$\mathbf{v}_{zz} = \frac{1}{\sqrt{2}} \begin{pmatrix} -1 \\ 1 \\ 0 \end{pmatrix}. \tag{5.0.1}$$

Hence, the spin vector for zz-bond on this minimum energy line can be written as

$$\begin{pmatrix} S^z_{\mathbf{k},1} \\ S^z_{\mathbf{k},2} \\ S^z_{\mathbf{k},3} \end{pmatrix} = \sqrt{2}\mathbf{v}_{zz}\delta_{\mathbf{k},\mathbf{M}_z}. \tag{5.0.2}$$

In real space, this gives us the following eigenvector

$$\begin{pmatrix} S^z_{\mathbf{r},1} \\ S^z_{\mathbf{r},2} \\ S^z_{\mathbf{r},3} \end{pmatrix} = e^{i\ \mathbf{M}_z \cdot\ \mathbf{r}} \begin{pmatrix} -1 \\ 1 \\ 0 \end{pmatrix}. \tag{5.0.3}$$

This state satisfies the spin length constraint on the first two sublattices but not on the third, so the LT method does not yet deliver a faithful minimum configuration. It turns out that we can solve this problem by noticing that there is another eigenvector

$$\mathbf{v'}_{zz} = \begin{pmatrix} 0 \\ 0 \\ 1 \end{pmatrix}. \tag{5.0.4}$$

with eigenvalue zero. This means that we can combine the two eigenvectors of the LT matrix and get the same total energy:

$$\begin{pmatrix} S'^z_{\mathbf{r},1} \\ S'^z_{\mathbf{r},2} \\ S'^z_{\mathbf{r},3} \end{pmatrix} = e^{i\ \mathbf{M}_z \cdot\ \mathbf{r}} \left[\begin{pmatrix} -1 \\ 1 \\ 0 \end{pmatrix} \pm \begin{pmatrix} 0 \\ 0 \\ 1 \end{pmatrix} \right]. \tag{5.0.5}$$

The free choice of the prefactor of ± 1 in front of the second eigenvector shows that the third sublattice is free to point up or down, without changing the energy.

This aspect gives rise to an extensive degeneracy of the ground state manifold. We now satisfy the LT constraint for every sublattice in $\mathbf{S'}^{z}(\mathbf{r})$ vector in (5.0.5).

2. $\Lambda^{y}(k)$ Matrix:

As it is indicated with the LT method, minimum energy solution for yy-bond is given as any point on the line $\mathbf{M}_y - \Gamma$ in BZ. See Fig.5.2 below.

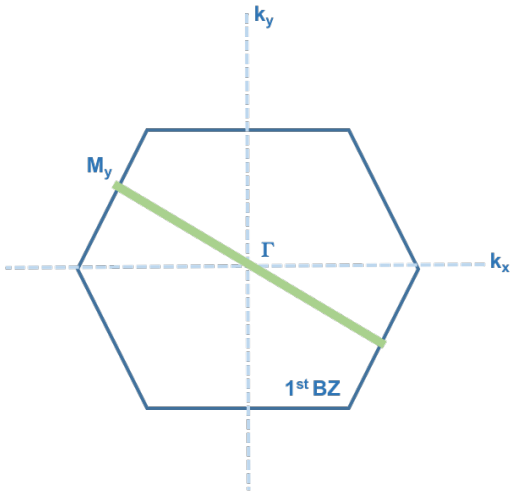

Figure 5.2: Minimum energy line on yy bond over the 1st BZ indicated.

For $\mathbf{k} = \mathbf{M}_y$, the minimum eigenvalue, λ_{min} corresponds to the eigenvector,

$$\mathbf{v}_{yy} = \frac{1}{\sqrt{2}} \begin{pmatrix} -1 \\ 0 \\ 1 \end{pmatrix}. \tag{5.0.6}$$

Hence, the spin vector for yy-bond on this minimum energy line can be written In reciprocal space as

$$\begin{pmatrix} S^{y}_{\mathbf{k},1} \\ S^{y}_{\mathbf{k},2} \\ S^{y}_{\mathbf{k},3} \end{pmatrix} = \sqrt{2}\mathbf{v}_{yy}\delta_{\mathbf{k},\mathbf{M}_y}. \tag{5.0.7}$$

In real space as

$$\begin{pmatrix} S^y_{\mathbf{r},1} \\ S^y_{\mathbf{r},2} \\ S^y_{\mathbf{r},3} \end{pmatrix} = e^{i\ \mathbf{M}_{\ y}\cdot\ \mathbf{r}}\ \begin{pmatrix} -1 \\ 0 \\ 1 \end{pmatrix}. \tag{5.0.8}$$

This state satisfies the spin length constraint on the first and third sublattices but not on the second, so the LT method does not yet deliver a faithful minimum configuration. It turns out that we can solve this problem by noticing that there is another eigenvector

$$\mathbf{v'}_{yy} = \begin{pmatrix} 0 \\ 1 \\ 0 \end{pmatrix}. \tag{5.0.9}$$

with eigenvalue zero. This means that we can combine the two eigenvectors of the LT matrix and get the same total energy:

$$\begin{pmatrix} S'^y_{\mathbf{r},1} \\ S'^y_{\mathbf{r},2} \\ S'^y_{\mathbf{r},3} \end{pmatrix} = e^{i\ \mathbf{M}_{\ y}\cdot\ \mathbf{r}}\ \left[\begin{pmatrix} -1 \\ 0 \\ 1 \end{pmatrix} \pm \begin{pmatrix} 0 \\ 1 \\ 0 \end{pmatrix} \right]. \tag{5.0.10}$$

Again, LT constraint is satisfied now for every sublattice in $\mathbf{S'}^y(\mathbf{r})$ vector in (5.0.10).

3. $\Lambda^x(k)$ Matrix:

As it is indicated with the LT method, minimum energy solution for xx-bond is given as any point on the line $\mathbf{M}_x - \Gamma$ in BZ. See Fig.5.3 below.

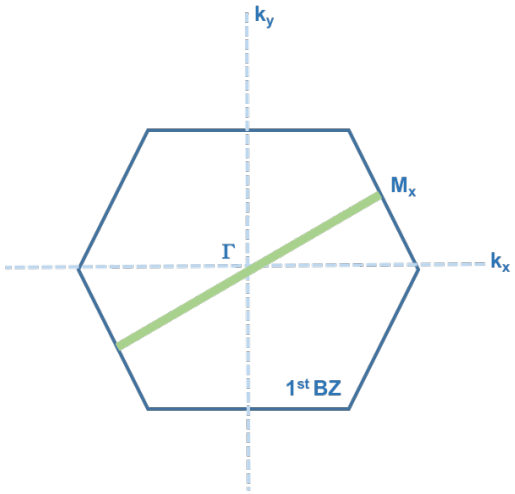

Figure 5.3: Minimum energy line on xx bond over the 1st BZ indicated.

For $\mathbf{k} = \mathbf{M}_x$, the minimum eigenvalue, λ_{min} corresponds to the eigenvector,

$$\mathbf{v}_{xx} = \frac{1}{\sqrt{2}} \begin{pmatrix} 0 \\ -1 \\ 1 \end{pmatrix}. \tag{5.0.11}$$

Hence, the spin vector for yy-bond on this minimum energy line can be written In reciprocal space as

$$\begin{pmatrix} S^x_{\mathbf{k},1} \\ S^x_{\mathbf{k},2} \\ S^x_{\mathbf{k},3} \end{pmatrix} = \sqrt{2}\mathbf{v}_{xx}\delta_{\mathbf{k},\mathbf{M}_x}. \tag{5.0.12}$$

In real space as

$$\begin{pmatrix} S^x_{\mathbf{r},1} \\ S^x_{\mathbf{r},2} \\ S^x_{\mathbf{r},3} \end{pmatrix} = e^{i\ \mathbf{M}_x \cdot\ \mathbf{r}} \begin{pmatrix} 0 \\ -1 \\ 1 \end{pmatrix}. \tag{5.0.13}$$

This state satisfies the spin length constraint on the second and third sublattices but not on the first, so the LT method does not yet deliver a faithful minimum

configuration. It turns out that we can solve this problem by noticing that there is another eigenvector

$$\mathbf{v'}_{xx} = \begin{pmatrix} 1 \\ 0 \\ 0 \end{pmatrix}. \tag{5.0.14}$$

with eigenvalue zero. This means that we can combine the two eigenvectors of the LT matrix and get the same total energy:

$$\begin{pmatrix} S'^{x}_{\mathbf{r},1} \\ S'^{x}_{\mathbf{r},2} \\ S'^{x}_{\mathbf{r},3} \end{pmatrix} = e^{i\ \mathbf{M}_{x}\cdot\ \mathbf{r}} \left[\begin{pmatrix} 0 \\ -1 \\ 1 \end{pmatrix} \pm \begin{pmatrix} 1 \\ 0 \\ 0 \end{pmatrix} \right]. \tag{5.0.15}$$

LT constraint is satisfied for every sublattice in $\mathbf{S'}^{x}(\mathbf{r})$ vector, (5.0.15), in this case as well.

Based on the eigenvector solutions, we can realize how frustration is observed in our model. See that in each eigenvector solution for each bond, we have -1,1, and 0 elements. Meaning, first two represents down and up spin respectively, while the latter one is a combination of both up and down spins and indicates frustration.

5.0.2 Eigenvectors for Heisenberg limit

Observe that in Heisenberg limit all $\Lambda(k)$ matrices are equal, and unlike Kitaev limit where minimum energy solutions corresponds to a line, any point inside the BZ will give minimum energy. Meaning, we have a flat band on the energy spectrum indicating infinitely many degenerate solutions.

In this section, we will demonstrate eigenvector solutions in different symmetry points on BZ, and see how they give exactly the same degenerate energy solution. So, first, lets start with Γ point, and then, proceed to $\mathbf{K}$ and $\mathbf{M}$ points on the 1st BZ.

1. $\mathbf{k} = \Gamma$

For this point we have two eigenvector solutions degenerate with the eigenenergy, which are

$$\begin{aligned}\mathbf{v}_1 &= \frac{1}{\sqrt{2}}\begin{pmatrix}-1\\0\\1\end{pmatrix}\\ \mathbf{v}_2 &= \frac{1}{\sqrt{2}}\begin{pmatrix}-1\\1\\0\end{pmatrix}, \forall\gamma = x, y, z.\end{aligned} \tag{5.0.16}$$

Since these two vectors in (5.0.16) aren't orthogonal to each other, we need to use Gram-Schmidt orthogonalization to make them orthogonal to each other. Resultant vectors then become

$$\begin{aligned}\mathbf{u}_1 &= \frac{1}{\sqrt{2}}\begin{pmatrix}-1\\0\\1\end{pmatrix}\\ \mathbf{u}_2 &= \frac{1}{\sqrt{6}}\begin{pmatrix}-1\\2\\-1\end{pmatrix}, \forall\gamma = x, y, z.\end{aligned} \tag{5.0.17}$$

Note that any linear combinations of the vectors in (5.0.17) will also give the eigenenergy solution in reciprocal space,

$$\begin{aligned}\begin{pmatrix}\mathbf{S}_{\mathbf{k},1}\\ \mathbf{S}_{\mathbf{k},2}\\ \mathbf{S}_{\mathbf{k},3}\end{pmatrix} &= u_1\hat{e}_1 + u_2\hat{e}_2\\ &= \begin{pmatrix}\frac{-\sqrt{3}}{2}\hat{e}_1 - \frac{1}{2}\hat{e}_2\\ \hat{e}_2\\ \frac{\sqrt{3}}{2}\hat{e}_1 - \frac{1}{2}\hat{e}_2\end{pmatrix}\delta_{\mathbf{k},\Gamma}.\end{aligned} \tag{5.0.18}$$

Where $\hat{e}_1$ and $\hat{e}_2$ are any two arbitrary orthonormal unit vectors that define the spin plane. Observe that this eigenvector solution corresponds to the Fig.5.4 below,

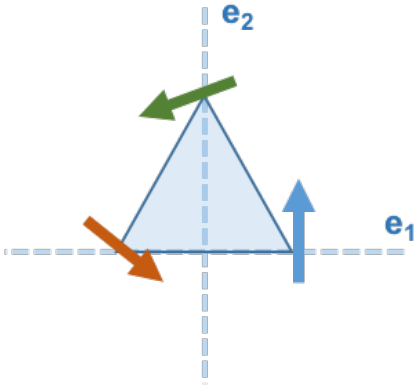

Figure 5.4: $\mathbf{k} = \Gamma$ eigenvector solution, preserving 120^0 state, for Heisenbergy limit is indicated, where e_1 and e_2 are unit vectors in spin spcace.

Where green color represents the first row, blue represents the second row and orange represents the last row in (5.0.18).

In real space, however, we have,

$$\begin{pmatrix} \mathbf{S}_{\mathbf{r},1} \\ \mathbf{S}_{\mathbf{r},2} \\ \mathbf{S}_{\mathbf{r},3} \end{pmatrix} = \begin{pmatrix} -\frac{\sqrt{3}}{2}\hat{e}_1 - \frac{1}{2}\hat{e}_2 \\ \hat{e}_2 \\ \frac{\sqrt{3}}{2}\hat{e}_1 - \frac{1}{2}\hat{e}_2 \end{pmatrix}. \tag{5.0.19}$$

2. $\mathbf{k} = \mathbf{K}_1 = (\frac{4\pi}{3}, 0)$ and $\mathbf{k} = \mathbf{K}_2 = (\frac{2\pi}{3}, \frac{2\pi}{\sqrt{3}})$.

$$\begin{pmatrix} \mathbf{S}_{\mathbf{K}_1,1} \\ \mathbf{S}_{\mathbf{K}_1,2} \\ \mathbf{S}_{\mathbf{K}_1,3} \end{pmatrix} = \begin{pmatrix} -\frac{\sqrt{1}}{2}\hat{e}_2 - \frac{\sqrt{3}}{2}\hat{e}_1 \\ -\frac{\sqrt{3}}{2}\hat{e}_1 + \frac{1}{2}\hat{e}_{2\hat{e}_2} \\ \hat{e}_2 \end{pmatrix} \delta_{\mathbf{k},\mathbf{K}_1}$$
$$\begin{pmatrix} \mathbf{S}_{\mathbf{K}_2,1} \\ \mathbf{S}_{\mathbf{K}_2,2} \\ \mathbf{S}_{\mathbf{K}_2,3} \end{pmatrix} = \begin{pmatrix} -\frac{\sqrt{1}}{2}\hat{e}_2 + \frac{\sqrt{3}}{2}\hat{e}_1 \\ -\frac{\sqrt{3}}{2}\hat{e}_1 - \frac{1}{2}\hat{e}_{2\hat{e}_2} \\ \hat{e}_2 \end{pmatrix} \delta_{\mathbf{k},\mathbf{K}_2}. \tag{5.0.20}$$

See Fig.5.5 for spin alignments,

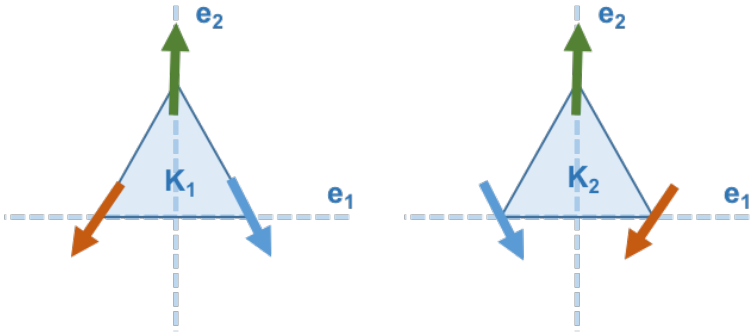

Figure 5.5: $\mathbf{k} = \mathbf{K}_1$ and $\mathbf{k} = \mathbf{K}_2$ eigenvector solutions, preserving 120^0 state, for Heisenbergy limit is indicated, where e_1 and e_2 are unit vectors in spin spcace.

In real space, however, we have,

$$\begin{pmatrix} \mathbf{S}_{\mathbf{r},1} \\ \mathbf{S}_{\mathbf{r},2} \\ \mathbf{S}_{\mathbf{r},3} \end{pmatrix} = e^{i\mathbf{K}_1.\mathbf{r}} \begin{pmatrix} -\frac{\sqrt{1}}{2}\hat{e}_2 - \frac{\sqrt{3}}{2}\hat{e}_1 \\ -\frac{\sqrt{3}}{2}\hat{e}_1 + \frac{1}{2}\hat{e}_{2\hat{e}_2} \\ \hat{e}_2 \end{pmatrix} + e^{i\mathbf{K}_2.\mathbf{r}} \begin{pmatrix} -\frac{\sqrt{1}}{2}\hat{e}_2 + \frac{\sqrt{3}}{2}\hat{e}_1 \\ -\frac{\sqrt{3}}{2}\hat{e}_1 - \frac{1}{2}\hat{e}_{2\hat{e}_2} \\ \hat{e}_2 \end{pmatrix}. \tag{5.0.21}$$

5.0.3 Classical phase diagram

Here we will analyze the classical phase diagram that we presented in Chapter-1, i.e. Fig.1.3. in detail.

With the help of the results obtained from the Luttinger-Tizsa method, we can easily comment on the phases for the Heisenberg, $J = cos(\phi)$, and Kitaev, $K = sin(\phi)$, limits at $0, \pi$ and $\pi/2, 3\pi/2$ respectively. So, for $\phi = 0$, we observe anti-ferromagnetic Heisenberg (AFMH) phase having SO(3) symmetry, while for $\phi = \pi$, we observe ferromagnetic Heisenberg (FMH) phase having SO(3) symmetry again. For $\phi = \pi/2$, we observe anti-ferromagnetic Kitaev (AFMK) phase, while for $\phi = 3\pi/2$, we observe ferromagnetic Kitaev (FMK) phase. Besides these specific points, we can further observe $\mathbf{q} = 0$ AFM and FM phases. We observe three more additional magnetically ordered phases on the phase diagram with the help of 3-sublattice transformation which was discussed in Chapter 4.

By using the duality transformation, we can decide on the boundaries of these phases on the phase diagram. After the rotation, we observe that Kitaev and Heisenberg points are self-dual, and $\mathbf{q} = 0$ AFM phase extends to a region for $\phi\epsilon(0, \arctan(-2) + \pi)$, while $\mathbf{q} = 0$ FM phase extends to a region for $\phi\epsilon(\pi, 3\pi/2)$. Additional to these phases, we set boundaries for another set of possible phases appearing on the phase diagram which we will decide what they are after we observe the states of these phases in detail with the help of LT results.

So, let's analyze the states appearing on the phase diagram one by one;

(a) $\phi = 0$

At this single point, which is self-dual under transformation, we observe $\mathbf{q} = 0$ HAFM order having SO(3) symmetry. States,which we already found in Sec.. 5.0.2, are infinitely degenerate, i.e. replicas of $\mathbf{q} = 0$ states, and we can see this degeneracy as a flat-band in the energy spectrum obtained with the LT method. Note that degeneracy associated with this state is related to the symmetry.

(b) $\phi\epsilon(0, \arctan(-2) + \pi) \;\; | \; \phi \neq \pi/2$

In this region, we observe eight $\mathbf{q} = 0$ AFM ordered coplanar states. In order to analyze these states better, we need to use the results of the eigenstate solutions from the LT method.

Note that we have 3 spin vectors representing the 3 different sublattices, and note also that each component of these spin vectors coming from different Λ-matrices, i.e. x,y,z. So, in order to write down a total spin vector we need to make a linear combination of the states that we obtained from the Λ-matrices as we divide and work on the Λ-matrices separately. After making the linear combination, we can, then, define the 3 different sublattice spin vectors explicitly.

$$\begin{pmatrix} \mathbf{S}_{\mathbf{r},1} \\ \mathbf{S}_{\mathbf{r},2} \\ \mathbf{S}_{\mathbf{r},3} \end{pmatrix} = \frac{c_x}{\sqrt{2}} \begin{pmatrix} 0 \\ -1 \\ 1 \end{pmatrix} \hat{x} + \frac{c_y}{\sqrt{2}} \begin{pmatrix} -1 \\ 0 \\ 1 \end{pmatrix} \hat{y} + \frac{c_z}{\sqrt{2}} \begin{pmatrix} 1 \\ -1 \\ 0 \end{pmatrix} \hat{z}. \tag{5.0.22}$$

Where that the linear combination coefficients must follow the condition,

$$\begin{aligned} \mathbf{S}^2_{\mathbf{r},1} &= (1/2)(-{c_y}^2 + {c_z}^2) = 1 \\ \mathbf{S}^2_{\mathbf{r},2} &= (1/2)(-{c_x}^2 + -{c_z}^2) = 1 \\ \mathbf{S}^2_{\mathbf{r},3} &= (1/2)({c_x}^2 + {c_y}^2) = 1 \\ |c_x| &= |c_y| = |c_z| = \pm 1. \end{aligned} \tag{5.0.23}$$

in order to preserve the spin length as unity for all sites.

Now we can represent sublattice spins as

$$\mathbf{S}_{\mathbf{r},1} = \frac{1}{\sqrt{2}} \begin{pmatrix} 0 \\ -c_y \\ c_z \end{pmatrix}, \mathbf{S}_{\mathbf{r},2} = \frac{1}{\sqrt{2}} \begin{pmatrix} -c_x \\ 0 \\ -c_z \end{pmatrix}, \mathbf{S}_{\mathbf{r},3} = \frac{1}{\sqrt{2}} \begin{pmatrix} c_x \\ c_y \\ 0 \end{pmatrix}, \forall r. \tag{5.0.24}$$

Note that there are 8 combinations of the coefficients which lead to 8 distinct ground states.

Note further that $\mathbf{S}_{\mathbf{r},1} \cdot [\mathbf{S}_{\mathbf{r},2} \times \mathbf{S}_{\mathbf{r},3}] = 0$, and similary, any combination of cyclic rotations gives the same result. Meaning, any choice of two sublattice spins lie on the same plane, that is coplanar.

(c) $\phi = \pi/2$

This point is also self-dual under transformation, and we observe KAFM order at this point. States, which we already found in Sec.5.0.1, are degenerate in accordance with the formula derived in Sec. 3.4.15, which obeys sliding symmetry.

(d) $\phi\epsilon(\arctan(-2) + \pi, \pi)$

This region is self-dual and we observe eight $\mathbf{q} = 0$ non-coplanar states. We will label this region as phase-A. In order to analyze these states better, we again need to use the results of the eigenstate solutions from LT method. We will follow the same procedure as in (2). The only difference is we cannot represent the eigenvector solutions as explicitly as in (2), but instead we will label the components as a and b, which both are real numbers and follow the same combination within the specified region.

$$\begin{pmatrix} \mathbf{S}_{\mathbf{r},1} \\ \mathbf{S}_{\mathbf{r},2} \\ \mathbf{S}_{\mathbf{r},3} \end{pmatrix} = \frac{c_x}{\sqrt{m}} \begin{pmatrix} b \\ a \\ a \end{pmatrix} \hat{x} + \frac{c_y}{\sqrt{m}} \begin{pmatrix} a \\ b \\ a \end{pmatrix} \hat{y} + \frac{c_z}{\sqrt{m}} \begin{pmatrix} a \\ a \\ b \end{pmatrix} \hat{z}, m = 2a^2 + b^2, \forall r. \tag{5.0.25}$$

So, we can represent sublattice spins as

$$\mathbf{S}_{\mathbf{r},1} = \frac{1}{\sqrt{m}} \begin{pmatrix} c_x b \\ c_y a \\ c_z a \end{pmatrix}, \mathbf{S}_{\mathbf{r},2} = \frac{1}{\sqrt{m}} \begin{pmatrix} c_x a \\ c_y b \\ c_z a \end{pmatrix}, \mathbf{S}_{\mathbf{r},3} = \frac{1}{\sqrt{m}} \begin{pmatrix} c_x a \\ c_y a \\ c_z b \end{pmatrix}, \forall r. \tag{5.0.26}$$

Note that $\mathbf{S}_{\mathbf{r},1} \cdot [\mathbf{S}_{\mathbf{r},2} \times \mathbf{S}_{\mathbf{r},3}] \neq 0$, and similary, any combination of cyclic rotations gives the same result. Meaning, any choice of two sublattice spins do not lie on the same plane this time, i.e. they are non-coplanar.

(e) $\phi = \pi$

This is another self-dual point, and we observe $\mathbf{q} = 0$ HFM order having SO(3) symmetry. States, which we already found in Sec.5.0.2 are infinitely degenerate, i.e. replicas of $\mathbf{q} = 0$ states, and we can see this degeneracy as a flat-band in the energy spectrum obtained with the LT method. Note that the states are ferromagnetically ordered in any direction and thus the degeneracy associated with these states is again related to the symmetry.

(f) $\phi\epsilon(\pi, 3\pi/2)$

In this region, we observe eight $\mathbf{q} = 0$ FM ordered states, which we can represent by following the same procedure as in (3),

$$\begin{pmatrix} \mathbf{S}_{\mathbf{r},1} \\ \mathbf{S}_{\mathbf{r},2} \\ \mathbf{S}_{\mathbf{r},3} \end{pmatrix} = \frac{c_x}{\sqrt{m}} \begin{pmatrix} -c \\ -d \\ -d \end{pmatrix} \hat{x} + \frac{c_y}{\sqrt{m}} \begin{pmatrix} d \\ c \\ d \end{pmatrix} \hat{y} + \frac{c_z}{\sqrt{m}} \begin{pmatrix} -d \\ -d \\ -c \end{pmatrix} \hat{z}, m = 2d^2 + c^2, \forall r. \tag{5.0.27}$$

So, we can represent sublattice spins as

$$\mathbf{S}_{\mathbf{r},1} = \frac{1}{\sqrt{m}} \begin{pmatrix} -c_x c \\ c_y d \\ -c_z d \end{pmatrix}, \mathbf{S}_{\mathbf{r},2} = \frac{1}{\sqrt{m}} \begin{pmatrix} -c_x d \\ c_y c \\ -c_z d \end{pmatrix}, \mathbf{S}_{\mathbf{r},3} = \frac{1}{\sqrt{m}} \begin{pmatrix} -c_x d \\ c_y d \\ -c_z c \end{pmatrix}, \forall r. \tag{5.0.28}$$

Where c and d are real numbers.

(g) $\phi\epsilon(3\pi/2, \arctan(-2))$

This region is self-dual and we observe eight $\mathbf{q} = 0$ non-coplanar states which are same as the 8 states appearing in region $[\arctan(-2) + \pi, \pi)$ but with different combinations. So, that's why we say the region is again self-dual but we will label this region as dual-non-coplanar state because it has the same 8 states as in non-coplanar state. In order to analyze these states better, we again need to use the results of the eigenstate solutions from LT method.
We will follow the same procedure as in (3) with e and f are real numbers.

$$\begin{pmatrix} \mathbf{S}_{\mathbf{r},1} \\ \mathbf{S}_{\mathbf{r},2} \\ \mathbf{S}_{\mathbf{r},3} \end{pmatrix} = \frac{c_x}{\sqrt{m}} \begin{pmatrix} e \\ -f \\ -f \end{pmatrix} \hat{x} + \frac{c_y}{\sqrt{m}} \begin{pmatrix} f \\ -e \\ f \end{pmatrix} \hat{y} + \frac{c_z}{\sqrt{m}} \begin{pmatrix} -f \\ -f \\ e \end{pmatrix} \hat{z}, m = 2f^2 + e^2, \forall r. \tag{5.0.29}$$

So, we can represent sublattice spins as

$$\mathbf{S}_{\mathbf{r},1} = \frac{1}{\sqrt{m}} \begin{pmatrix} c_x e \\ c_y f \\ -c_z f \end{pmatrix}, \mathbf{S}_{\mathbf{r},2} = \frac{1}{\sqrt{m}} \begin{pmatrix} -c_x f \\ -c_y e \\ -c_z f \end{pmatrix}, \mathbf{S}_{\mathbf{r},3} = \frac{1}{\sqrt{m}} \begin{pmatrix} -c_x f \\ c_y f \\ c_z e \end{pmatrix}. \tag{5.0.30}$$

To see that this region is also self-dual, we apply 3-sublattice transformation on the states in and compare them with (5.0.29). If the real numbers, i.e. c and d, follow the same sequence as in (5.0.29), then they are self-dual, but if not, then we say solutions belong to the same set but with differently combined, and that's why the region is self-dual.
So, if we apply (4.0.1) on (5.0.33), we obtain,

$$\tilde{\mathbf{S}}_{\mathbf{r},1} = \frac{1}{\sqrt{m}} \begin{pmatrix} -c_x e \\ c_y f \\ c_z f \end{pmatrix}, \tilde{\mathbf{S}}_{\mathbf{r},2} = \frac{1}{\sqrt{m}} \begin{pmatrix} -c_x f \\ c_y e \\ c_z f \end{pmatrix}, \tilde{\mathbf{S}}_{\mathbf{r},3} = \frac{1}{\sqrt{m}} \begin{pmatrix} -c_x f \\ c_y f \\ c_z e \end{pmatrix}, \forall r. \tag{5.0.31}$$

We see that transformed spin vectors has the same set of solutions but follow a different sequence. So, this makes the region self-dual.

(h) $\phi = 3\pi/2$

This point is also self-dual under transformation, and we observe KFM order at this point. States, which we already found in Sec.5.0.1, are degenerate in accordance with the formula derived in Sec. 3.4.15, which obeys sliding symmetry.

(i) $\phi\epsilon(\arctan(-2) + \pi, 2\pi)$

In this region, we observe eight $\mathbf{q} = 0$ dual-FM ordered states, which we can represent by following the same procedure as in (3),

$$\begin{pmatrix} \mathbf{S}_{\mathbf{r},1} \\ \mathbf{S}_{\mathbf{r},2} \\ \mathbf{S}_{\mathbf{r},3} \end{pmatrix} = \frac{c_x}{\sqrt{m}} \begin{pmatrix} g \\ -h \\ -h \end{pmatrix} \hat{x} + \frac{c_y}{\sqrt{m}} \begin{pmatrix} h \\ -g \\ h \end{pmatrix} \hat{y} + \frac{c_z}{\sqrt{m}} \begin{pmatrix} -h \\ -h \\ g \end{pmatrix} \hat{z}, m = 2h^2 + g^2, \forall r. \tag{5.0.32}$$

So, we can represent sublattice spins as

$$\mathbf{S}_{\mathbf{r},1} = \frac{1}{\sqrt{m}} \begin{pmatrix} c_x g \\ c_y h \\ -c_z h \end{pmatrix}, \mathbf{S}_{\mathbf{r},2} = \frac{1}{\sqrt{m}} \begin{pmatrix} -c_x h \\ -c_y g \\ -c_z h \end{pmatrix}, \mathbf{S}_{\mathbf{r},3} = \frac{1}{\sqrt{m}} \begin{pmatrix} -c_x h \\ c_y h \\ c_z g \end{pmatrix}, \forall r. \tag{5.0.33}$$

Where g and h are again real numbers.

To see that this region is also self-dual or not, we apply 3-sublattice transformation on these states and compare them with (5.0.31). If the real numbers, i.e. c and d, follow the same sequence as in (5.0.31), then they are self-dual. So, if we apply (4.0.1) on (5.0.33), we obtain,

$$\tilde{\mathbf{S}}_{\mathbf{r},1} = \frac{1}{\sqrt{m}} \begin{pmatrix} -c_x g \\ c_y h \\ c_z h \end{pmatrix}, \tilde{\mathbf{S}}_{\mathbf{r},2} = \frac{1}{\sqrt{m}} \begin{pmatrix} -c_x h \\ c_y g \\ c_z h \end{pmatrix}, \tilde{\mathbf{S}}_{\mathbf{r},3} = \frac{1}{\sqrt{m}} \begin{pmatrix} -c_x h \\ c_y h \\ c_z g \end{pmatrix}, \forall r. \tag{5.0.34}$$

We see that transformed spin vectors has exactly the same sequence of solutions. So, we see that this is a dual region of (9).

Fig.1.3 summarizes the phases we covered in this section. At $\phi = 0$, system has HAFM ordered state with infinite degeneracy having $SO(3)$ spin symmetry. Within a range of $\phi\epsilon(0, \arctan(-2) + \pi)$, system shows $\mathbf{q} = 0$ coplanar AFM ordered state with accidental degeneracy. Note that this phase is self-dual. At $\phi = \pi/2$, system has KAFM ordered state with degeneracy defined on Chapter-2. Within a range of $\phi\epsilon(\arctan(-2) + \pi, \pi)$, system shows eight $\mathbf{q} = 0$ non-coplanar states with accidental degeneracy. Note that the point $\phi = \arctan(-2) + \pi$ is doubly degenerate with 120^o and 60^o states. So for $a = b$, system shows coplanar configuration at this point instead of non-coplanar configuration. At $\phi = \pi$, system has HFM ordered state with infinite degeneracy having $SO(3)$ spin symmetry. Within a range of $\phi\epsilon(\pi, 3\pi/2)$, the system shows eight $\mathbf{q} = 0$ FM ordered states with accidental degeneracy. At $\phi = 3\pi/2$, system has KFM ordered state with degeneracy defined on Chapter-3. Within a range of $\phi\epsilon(3\pi/2, \arctan(-2))$, system shows eight $\mathbf{q} = 0$ non-coplanar states with accidental degeneracy. Note that this phase is again self-dual but shares the same set of solutions as the $\mathbf{q} = 0$ coplanar states. Within a range of $\phi\epsilon(\arctan(-2), 2\pi)$, system shows eight $\mathbf{q} = 0$ FM ordered states. Note that this phase is a dual of $\mathbf{q} = 0$ FM ordered states.

Chapter 6

Discussion

In this thesis, we analayzed the classical phase diagram, Fig.1.3, of Kitaev-Heisenberg model on the kagome lattice.

First we diagonalize the Λ-matrices by using the LT method. We see that the LT method works in each case and the solution found with a weak constraint also satisfies the strong constraint which requires to preserve spin length at each site. This is our advantage as we only need to deal with the single linear constraint equation to obtain the whole eigenstates and eigenvalues for the ground state configuration.

We observed that the minimum energy configurations are highly degenerate with both linear, coplanar, and non-coplanar solutions, which is a feature of the frustrated spin systems. Analyzing these ground state solutions helped us to draw the full classical phase diagram for this system.

After applying the three sublattice transformation, we observed that there exists five phases on the classical phase diagram in which two regions are duals of each other, while others are self dual. It is interesting to see that among infinitely many degenerate ground state configurations some are selected depending on the strength of the interactions, K and J.

We only covered nearest neighbor (n.n.) interactions on kagome lattice in consideration of the classical regime. Thus, it might be interesting to consider the

quantum regime having the long-range interactions. This will done in a future study.

References

[1] P. W. Anderson. The resonating valence bond state in la2cuo4 and superconductivity. *Science*, 235(4793):1196–1198, 1987.

[2] Leon Balents. Spin liquids in frustrated magnets. *Nature*, 464(7286):199–208, 03 2010.

[3] R. J. Baxter. Colorings of a hexagonal lattice. *Journal of Mathematical Physics*, 11(3):784–789, 1970.

[4] Ji ří Chaloupka, George Jackeli, and Giniyat Khaliullin. Kitaev-heisenberg model on a honeycomb lattice: Possible exotic phases in iridium oxides A_2iro$_3$. *Phys. Rev. Lett.*, 105:027204, Jul 2010.

[5] Ji ří Chaloupka, George Jackeli, and Giniyat Khaliullin. Kitaev-heisenberg model on a honeycomb lattice: Possible exotic phases in iridium oxides A_2iro$_3$. *Phys. Rev. Lett.*, 105:027204, Jul 2010.

[6] Gang Chen and Leon Balents. Spin-orbit coupling in d^2 ordered double perovskites. *Phys. Rev. B*, 84:094420, Sep 2011.

[7] A. L. Chernyshev. Strong quantum effects in an almost classical antiferromagnet on a kagome lattice. *Phys. Rev. B*, 92:094409, Sep 2015.

[8] A. L. Chernyshev and M. E. Zhitomirsky. Order and excitations in large $-$ s kagome-lattice antiferromagnets. *Phys. Rev. B*, 92:144415, Oct 2015.

[9] Andrey Chubukov. Order from disorder in a kagomé antiferromagnet. *Phys. Rev. Lett.*, 69:832–835, Aug 1992.

[10] Tyler Dodds, Ting-Pong Choy, and Yong Baek Kim. Interplay between lattice distortion and spin-orbit coupling in double perovskites. *Phys. Rev. B*, 84:104439, Sep 2011.

[11] Lewis J. Downie, Elena I. Ardashnikova, Chiu C. Tang, Alexandre N. Vasiliev, Peter S. Berdonosov, Valery A. Dolgikh, Mark A. de Vries, and Philip Lightfoot. Novel s = 1/2 kagome lattice materials: Cs2ticu3f12 and rb2ticu3f12. *Crystals*, 5(2):226, 2015.

[12] David A. Huse and Andrew D. Rutenberg. Classical antiferromagnets on the kagomé lattice. *Phys. Rev. B*, 45:7536–7539, Apr 1992.

[13] L. B. Ioffe, M. V. Feigel'man, A. Ioselevich, D. Ivanov, M. Troyer, and G. Blatter. Topologically protected quantum bits using josephson junction arrays. *Nature*, 415(6871):503–506, 01 2002.

[14] G. Jackeli and G. Khaliullin. Mott insulators in the strong spin-orbit coupling limit: From heisenberg to a quantum compass and kitaev models. *Phys. Rev. Lett.*, 102:017205, Jan 2009.

[15] S. Janson. Roots of polynomials of degrees 3 and 4. *ArXiv e-prints*, September 2010.

[16] T. A. Kaplan and N. Menyuk. Spin ordering in three-dimensional crystals with strong competing exchange interactions. *Philosophical Magazine*, 87(25):3711–3785, 2007.

[17] Itamar Kimchi and Ashvin Vishwanath. Kitaev-heisenberg models for iridates on the triangular, hyperkagome, kagome, fcc, and pyrochlore lattices. *Phys. Rev. B*, 89:014414, Jan 2014.

[18] Alexei Kitaev. Anyons in an exactly solved model and beyond. *Annals of Physics*, 321(1):2 – 111, 2006. January Special Issue.

[19] K. I. Kugel' and D. I. Khomskii. The jahn-teller effect and magnetism: transition metal compounds. *Physics-Uspekhi*, 25(4):231–256, 1982.

[20] Patrick A. Lee, Naoto Nagaosa, and Xiao-Gang Wen. Doping a mott insulator: Physics of high-temperature superconductivity. *Rev. Mod. Phys.*, 78:17–85, Jan 2006.

[21] K. Li, S.-L. Yu, and J.-X. Li. Global phase diagram, possible chiral spin liquid, and topological superconductivity in the triangular Kitaev-Heisenberg model. *New Journal of Physics*, 17(4):043032, April 2015.

[22] D.B. Litvin. The luttinger-tisza method. *Physica*, 77(2):205 – 219, 1974.

[23] J. M. Luttinger and L. Tisza. Theory of dipole interaction in crystals. *Phys. Rev.*, 70:954–964, Dec 1946.

[24] P. Nikolic and T. Senthil. Physics of low-energy singlet states of the kagome lattice quantum heisenberg antiferromagnet. *Phys. Rev. B*, 68:214415, Dec 2003.

[25] H. F. Pen, J. van den Brink, D. I. Khomskii, and G. A. Sawatzky. Orbital ordering in a two-dimensional triangular lattice. *Phys. Rev. Lett.*, 78:1323–1326, Feb 1997.

[26] M. Schmidt, W. Ratcliff, P. G. Radaelli, K. Refson, N. M. Harrison, and S. W. Cheong. Spin singlet formation in $mgti_2o_4$: Evidence of a helical dimerization pattern. *Phys. Rev. Lett.*, 92:056402, Feb 2004.

[27] Rajiv R. P. Singh and David A. Huse. Ground state of the spin-1/2 kagome-lattice heisenberg antiferromagnet. *Phys. Rev. B*, 76:180407, Nov 2007.

[28] F. Trousselet, A. M. Ole?, and P. Horsch. Compass-heisenberg model on the square lattice ?spin order and elementary excitations. *EPL (Europhysics Letters)*, 91(4):40005, 2010.

[29] Hirokazu Tsunetsugu and Yukitoshi Motome. Magnetic transition and orbital degrees of freedom in vanadium spinels. *Phys. Rev. B*, 68:060405, Aug 2003.

[30] Chen Zeng and Veit Elser. Numerical studies of antiferromagnetism on a kagomé net. *Phys. Rev. B*, 42:8436–8444, Nov 1990.